Rego, S., Heal, T. J., Pidwill, G. R., Till, M., Robson, A., Lamont, R., ... Nobbs, A. H. (2016). Structural and Functional Analysis of Cell Wall-Anchored PolypeptideAdhesin BspA in Streptococcus agalactiae. Journal of Biological Chemistry, 291(31), 15985-16000. DOI: 10.1074/jbc.M116.726562

Structural and Functional Analysis of Cell Wall-Anchored Polypeptide Adhesin BspA in *Streptococcus agalactiae*

Sara Rego[‡§], Timothy J. Heal[§¶], Grace R. Pidwill[‡], Marisa Till[§||], Alice Robson[§], Richard J. Lamont[**], Richard B. Sessions[§||], Howard F. Jenkinson[‡], Paul R. Race[§||1], and Angela H. Nobbs[‡2]

From [‡]School of Oral & Dental Sciences, University of Bristol, UK; [§]School of Biochemistry, University of Bristol, UK; [¶]Bristol Centre for Functional Nanomaterials, University of Bristol, UK; [||]BrisSynBio Synthetic Biology Research Centre, University of Bristol, UK; [**]Department of Oral Immunology and Infectious Diseases, University of Louisville, USA

Running title: *Streptococcus agalactiae* BspA

To whom correspondence should be addressed: [1]Dr. Paul R. Race, School of Biochemistry, University of Bristol, Biomedical Sciences Building, University Walk, Bristol BS8 1TD, UK, Telephone: +44 (0)1173311835, Email: Paul.Race@bristol.ac.uk. [2]Dr. Angela H. Nobbs, School of Oral & Dental Sciences, University of Bristol, Lower Maudlin Street, Bristol, BS1 2LY, UK, Telephone:+44 (0)1173424779, Email: Angela.Nobbs@bristol.ac.uk.

Keywords: adhesin, AgI/II polypeptide, *Streptococcus*, virulence factor, *Candida albicans*, crystallography, circular dichroism (CD), isothermal titration calorimetry (ITC), molecular dynamics

ABSTRACT

Streptococcus agalactiae (Group B *Streptococcus*, GBS) is the predominant cause of early-onset infectious disease in neonates and is responsible for life threatening infections in elderly and immune-compromised individuals. Clinical manifestations of GBS infection include sepsis, pneumonia and meningitis. Here we describe BspA, a deviant antigen I/II family polypeptide that confers adhesive properties linked to pathogenesis in GBS. Heterologous expression of BspA on the surface of the non-adherent bacterium *Lactococcus lactis* confers adherence to scavenger receptor gp340, human vaginal epithelium, and to the fungus *Candida albicans*. Complementary crystallographic and biophysical characterization of BspA reveal a novel β-sandwich adhesion domain and unique asparagine-dependent super-helical stalk. Collectively these findings establish a new bacterial adhesin structure that has in effect been hijacked by a pathogenic *Streptococcus* species to provide competitive advantage in human mucosal infections.

Streptococcus agalactiae (Group B *Streptococcus*, GBS) is a commensal of the gastrointestinal tract and part of the normal microbiota of the female rectovaginal tract, where it is carried asymptomatically by approximately 10-40% of women of childbearing age (1). However, as an opportunistic pathogen, GBS is the leading cause of neonatal meningitis and sepsis in the developed world. The predominant route by which GBS is transmitted to infants is from the mother, either during birth or following breach of the placental barrier *in utero.* Antenatal GBS screening strategies are therefore commonly used to identify colonized women, who then receive antimicrobial prophylaxis. Nevertheless, GBS remains a major cause of morbidity and mortality in infants worldwide (2).

Since maternal GBS colonization is the primary risk factor for vertical transmission of neonatal infection (3) there has been considerable focus on the mechanisms underlying GBS colonization of the female genitourinary (GU) tract. A number of putative colonization determinants have been identified including: alpha C protein, mediating entry of GBS into cervical epithelial cells (4); pili, shown to contribute to vaginal attachment (5); and Srr-1, which binds keratin-4 (5) and fibrinogen (6) on the surface of vaginal epithelium. In addition, GBS expresses numerous extracellular

matrix (ECM)-binding proteins, including C5a peptidase (ScpB) and FbsA, which may promote attachment to mucosal tissues of the GU tract (7).

Antigen I/II (AgI/II) family polypeptide adhesins are found widely across the *Streptococcus* genus and have been best characterized for those streptococci indigenous to the oral cavity (8). *In silico* analyses have recently revealed the presence of genes encoding AgI/II family polypeptides in GBS, which we have designated here Group B *Streptococcus* surface proteins (Bsp). These proteins conform to a conserved primary structure consisting of seven distinct regions (Fig 1). The N-terminal region comprises a signal (leader) peptide, an N-terminal domain and an alanine-rich repeat region (A). The C-terminal region consists of a proline-rich repeat sequence (P) followed by a C-terminal domain (C) and an LPxTG motif required for bacterial cell wall anchorage. The A and P regions flank a central variable region (V), which exhibits the greatest strain-to-strain sequence variation between streptococci and is thought to confer ligand-binding specificity (8). Structural characterization of AgI/II family proteins from *Streptococcus mutans* (SpaP) and *Streptococcus gordonii* (SspB) has revealed a distinctive extended fibrillar structure that projects outwards from the wall-proximal C domain (Fig 1). The stalk is generated by a high affinity interaction between the α- and polyproline II (PPII)- helices of the A and P domains respectively, serving to present the V 'head' domain at its tip (9). The N-terminus forms a stabilizing scaffold by wrapping behind the base of the stalk (10). Crystal structures of the V regions of SpaP and SspB have revealed a common architecture consisting of a lectin-like fold with a putative binding cleft (11,12). The structure of the C-terminal subdomains C1, C2 and C3 has also been elucidated by X-ray crystallography and found to consist of β-sandwich domains stabilized by isopeptide bonds (13-16).

AgI/II family polypeptides are multifunctional adhesins that serve as important colonization determinants for oral streptococci, mediating binding to host substrata and to other resident microbes. A common receptor for AgI/II polypeptides is glycoprotein-340 (gp340), an innate immunity scavenger receptor produced at mucosal surfaces (17). Fluid-phase gp340, in saliva and other mucosal secretions, agglutinates microbes for clearance from the body, while solid-phase gp340 adsorbed onto host surfaces provides a substratum for microbial adherence (18). AgI/II family polypeptides have also been shown to promote microbial community development by binding to oral bacteria *Actinomyces oris* (19-21) or *Porphyromonas gingivalis* (22,23), as well as to the pathogenic fungus *Candida albicans* (24). More recently an AgI/II family polypeptide (AspA) has been described in Group A *Streptococcus* (GAS) (25). The gene encoding AspA is located within an Integrative and Conjugative Element (ICE) designated Region of Difference 2 (RD2), which is found amongst GAS serotypes implicated in puerperal fever (26,27). There is strong evidence that RD2 originated in GBS and was acquired by GAS through horizontal gene transfer. It has been proposed that genes carried within RD2 might contribute to both GAS and GBS pathogenicity (28,29). Supporting this, AspA has been shown to facilitate GAS biofilm formation on salivary pellicle (25), respiratory infection, and evasion of phagocytosis (30). Given this precedent, we hypothesized that Bsp polypeptides may serve as important host colonization determinants of GBS.

In this study we introduce four similar, but non-identical, Bsp family proteins that are distributed amongst GBS of different capsular serotypes. Crystallographic and biophysical characterization of isolated functional domains from one of these proteins (BspA) identifies unique structural features that distinguish it as an AgI/II family deviant. These findings are of significance in directing the development of new vaccines or anti-infective agents that selectively target GBS, whilst not impacting the commensal microbiota.

RESULTS

Distribution of AgI/II polypeptides in GBS

In silico analyses were undertaken to determine the prevalence of *bsp* genes across GBS, using the completed GBS genome sequences available on NCBI. *bsp* genes were found in five strains (summarized in Table 1), and each was present on a RD2-like ICE (28). Based upon primary sequence identities, four homologues of the *bsp* gene were identified, which we designated *bspA-D* (Fig 1B). BspA shares 90.35% amino acid (aa) sequence identity with BspB, and both homologues were found in strain NEM316, which carries one copy of *bspA* and three copies of *bspB*. The remaining GBS strains carry either *bspC* or *bspD*. The proteins

encoded by these genes share 99.52 - 99.76% aa sequence identity, with the only major difference being that BspD is missing a leader peptide (39-41 aa residues) for targeting to the Sec translocation machinery. BspA/B homologues can be separated from BspC/D homologues based upon the presence of two additional sequences in BspA/B homologues, one in the A domain (51 aa residues) and the second in the P domain (25 aa residues). There was no correlation between GBS capsular serotype and *bsp* homologue distribution.

BspA promotes binding to immobilized gp340

To investigate the functions of BspA as a putative colonization determinant in the absence of confounding problems due to adhesin redundancy in GBS, *L. lactis* was utilized as a heterologous expression strain. The *bspA* gene was cloned under control of a nisin-inducible promoter into vector pMSP (31), enabling expression of BspA to be regulated by the concentration of nisin added to the growth medium. Expression of BspA on the surface of *L. lactis* following nisin induction was confirmed by immuno-dot blot analysis (Fig 2A) with α-Spy1325mid antibodies to *S. pyogenes* AspA mid-region (25), which shares 63% aa sequence identity across corresponding $VPC_{473-990}$ region of BspA.

A primary host factor recognized by members of the AgI/II polypeptide family in oral streptococci and GAS is gp340, a mucin-like glycoprotein associated with the surface of mucosal tissues (17). When gp340 becomes adsorbed onto a surface, exposed cryptitopes can provide receptors for microbial adherence. To examine the interaction of BspA with gp340, binding levels of *L. lactis* expressing BspA (pMSP.$bspA^+$) to immobilized gp340 were compared to *L. lactis* containing empty vector (pMSP), using a crystal violet spectrophotometric assay. Adhesion levels of *L. lactis* pMSP.$bspA^+$ were significantly ($P < 0.005$) higher than those of *L. lactis* containing empty vector (Fig 2B). Furthermore, a dose-dependent response in binding to gp340 by BspA was seen with increasing nisin concentration. By contrast, neither *L. lactis* expressing BspA nor empty vector adhered to the blocking agent, bovine serum albumin (BSA).

There is evidence that the head (V) regions of SspB, SpaP and AspA facilitate gp340-binding activity (9,25,32). To determine if the V domain of BspA plays a similar role in mediating binding to immobilized gp340, anti-V domain antibodies were affinity-purified from α-Spy1325mid antiserum (Fig 3A). These antibodies (designated α-rV.BspA) were then investigated for capacity to impair adherence of *L. lactis* pMSP.$bspA^+$ to immobilized gp340. *L. lactis* expressing AgI/II family polypeptide SspB from *S. gordonii* was included as a control to confirm antiserum specificity. Lactococcal cells were labelled with FITC and binding to gp340 was measured using a fluorescence plate reader. Adherence of *L. lactis* pMSP.$bspA^+$ cells to immobilized gp340 was significantly ($P < 0.0001$) impaired by α-rV.BspA, which reduced binding by 85% relative to the no antiserum control (Fig 3B). Importantly, this inhibition was specific to the reactivity of α-rV.BspA antibody with BspA, as α-rV.BspA had no significant inhibitory effect on adherence of *L. lactis* pKS80.$sspB^+$ to immobilized gp340 (Fig 3B).

BspA interacts with C. albicans

Previous studies have shown that SspB expressed by *S. gordonii*, an integral member of the human oral microbiota, interacts with *C. albicans* hyphal cell wall Als3 protein, promoting the development of mixed species communities (24). *C. albicans* co-exists with GBS in the lower female GU tract, and several studies have observed recurrent co-isolation of GBS with *C. albicans* (33-35). To confirm the capacity for GBS to interact with *C. albicans*, FITC-labelled GBS NEM316 cells were incubated in suspension with hypha-forming cells of *C. albicans* SC5314 labelled with Calcofluor white, and aggregates were visualized by fluorescence microscopy. As reported for a number of oral streptococci (24,36-38), GBS NEM316 was shown to intimately interact with candidal cells, preferentially targeting *C. albicans* hyphal filaments rather than blastospores (Fig 4A). To determine if BspA was involved in promoting this association of GBS with *C. albicans*, the interactions of *L. lactis* expressing BspA or vector control (pMSP) with *C. albicans* were compared. *L. lactis* pMSP cells exhibited few interactions with *C. albicans* (Fig 4B). Similarly, uninduced *L. lactis* pMSP.$bspA^+$ cells associated only sparsely with candidal hyphae (Fig 4C). By contrast, *L. lactis* cells induced to express BspA showed high affinity for *C. albicans*, and preferentially bound along the lengths of the hyphal filaments (Fig 4C).

BspA promotes adhesion to human vaginal epithelium

GBS colonization of vaginal and cervical epithelia is the primary risk factor for vertical transmission of neonatal infection (3). To determine if BspA was a candidate for mediating GBS adherence to epithelial cells, binding levels of *L. lactis* pMSP.*bspA*$^+$ to a vaginal epithelial cell line, VK2/E6E7, were compared to those of *L. lactis* pMSP vector control. Lactococci were incubated with VK2/E6E7 monolayers and numbers of associated bacteria enumerated by viable count. Numbers of *L. lactis* cells expressing BspA associating with VK2/E6E7 monolayers were significantly ($P < 0.05$) higher than vector control (Fig 5), implying that BspA mediates adhesion to vaginal epithelial cells.

BspA possesses a truncated C-terminal domain that lacks bound metal ions

To gain further insight into the adhesive properties of BspA we sought to structurally characterize this protein. Initially we focused our efforts on the BspA C-terminal domain (BspA-C, 328 aa residues). Although our whole cell binding studies identify the BspA variable domain as being responsible for gp340 binding by this polypeptide, a role for the C-terminal domain of AgI/II family polypeptides in target binding has been suggested by others (9,15,39). Despite being significantly shorter (328 aa residues as compared to 502-508 aa in other AgI/II family proteins), BspA-C domain exhibits a high degree of sequence identity to equivalent regions in other AgI/II family proteins, indicative of analogous function. The crystal structures of BspA-C and a more readily crystallizable point mutant of this protein, BspA-C_{G744D} (both comprising residues 554-881 of full length BspA), were determined by molecular replacement in the space groups $C2_122$ and $P2_12_12_1$ respectively. The structure of BspA-C_{G744D} was determined to 1.8 Å resolution using the SspB-$C_{1083\text{-}1413}$ crystal structure (13) (PDB code 2WOY, 33% sequence identity) as a molecular replacement search model, and refined to a R_{work}/R_{free} of 19.6/23.4%. The structure of BspA-C domain was determined to 2.2 Å resolution using the BspA-C_{G744D} structure as a molecular replacement search model and refined to a R_{work}/R_{free} of 21.8/23.9%. For both BspA-C_{G744D} and BspA-C, the asymmetric unit comprises a single monomer of each protein. Crystal packing analysis reveals that Asp744 of BspA-C_{G744D} forms a salt bridge with Lys855 in symmetry-related molecules. This interaction is likely to account for the increased propensity of BspA-C_{G744D} to crystallize as compared to BspA-C. There are no significant structural differences between BspA-C_{G744D} and BspA-C structures, with a Cα RMSD between the two structures of 0.5 Å (255 atoms).

The final models of BspA-C_{G744D} (334 aa residues, including 6 residues of the N-terminal vector encoded hexapeptide) and BspA-C (311 aa residues, lacking aa residues 640-657) are presented in Fig 6A and comprise a pair of compact subdomains (residues 554-725 and 726-881 of full-length BspA) fused by a linker. The two subdomains are equivalent to those termed C2 and C3 in other AgI/II family polypeptides (13-16). The absence of a C1 subdomain, a feature that is present in all other AgI/II family proteins characterized to date, accounts for the size disparity between BspA-C domain and other AgI/II family C domains. The C1-C2 interface region has been suggested as having a role in carbohydrate binding in the *S. mutans* AgI/II family protein SpaP (15). Its absence in BspA, and by inference from sequence analysis of BspB-D (Fig 1B) reveals that this interface region is not required for target ligand recognition or binding in Bsp family members.

The two BspA-C subdomains consist of two central β-sheets, S1 and S2 in C2, and S3 and S4 in C3. S1 and S2 comprise four and five strands respectively. Strands β2 and β3 are connected by two short helices α1 and α2. Helix α6 runs parallel to α1 and α2 and connects β6 and β7. Helix α5 protrudes from the core of the C2 subdomain connecting strands β5 and β6. Similarly to S1 and S2, the β-sheets S3 and S4 contain four and five strands respectively. Long loops connect strands at the interface of the C2 and C3 subdomains. Helix α7 connects strands β17 and β18. Strands β13 and β16 are connected by two short anti-parallel strands β14 and β15. Connecting loops are shorter on the opposite side of the sandwich, except for a long coiled region connecting β10 and β11. C2 and C3 are connected by a long loop between strands β9 and β10. Protein-protein interactions at the C2-C3 interface region are stabilized by a series of hydrogen bonds. Both C2 and C3 possess a single isopeptide bond (Fig 6A). In C2 this is formed between the side chains Lys556 (NZ) and Asn703 (CG), and fuses S1 to S2. In C3 isopeptide bond formation occurs between Lys730 (NZ) and Asn861 (CG), linking S3 to S4.

Previously reported crystal structures of AgI/II family polypeptide C-terminal domains have identified the presence of bound metal ions, which have been suggested to play a role in enhancing stability and conferring adhesive properties (13-16). By contrast no bound metal ions are observed in the crystal structures of BspA-C_{G744D} or BspA-C. BspA-C2 subdomain does possess a putative unoccupied metal binding site, equivalently positioned to those reported in SpaP-C2, SspB-C2 and AspA-C2. This site lies at the interface of the loop regions that connect β3 to β4 and β6 to α5, and comprises the residues Gln-607, Pro-608, Val-659 and Glu-661. There is notable sequence disparity in the region of BspA-C3 that corresponds to the SpaP-C3 metal ion-binding site. The residues Asp1388 and Gln1391 in SpaP-C3, which act to coordinate a bound calcium ion, are found to be histidines in BspA-C3 (His-777 and His-780). In the AspA-C3 crystal structure (16) a single histidine substitution at the second of these positions (His-1205) appears sufficient to preclude metal ion binding.

The BspA variable domain possesses a β-sandwich fold that is structurally distinct from other AgI/II family polypeptides

Having established the role of the BspA variable domain in gp340 binding we next sought to determine the crystal structure of this region of the protein. The structure of the BspA variable domain (BspA-V, comprising aa residues 285-451 of the full length protein) was determined in space group *C*2 using the SAD technique, as applied to crystals of SeMet labelled BspA-V. The structure was determined to a resolution of 2.4 Å and refined to a R_{work}/R_{free} of 23.5/26.2%. The asymmetric unit contains two copies of BspA-V arranged in the form of a strand-swapped homodimer (Fig 6B). BspA dimerization results from the exchange of the C-terminal β-strand (residues 436-606) of each monomer within the dimer. In full length BspA the N- and C-termini of the V domain are fused to their neighboring A and P domains (Fig 1A), an organization that would preclude BspA-V domain strand-swapping and implies that dimerization is an artifact of crystallization. The positioning of the exchanged C-terminal strands are however indicative of their location within the parent monomer. There are no significant structural differences between the monomers within the dimer, with an RMSD Cα between the two of 0.9 Å (141 atoms). Convincing electron density was not observed for residues 14-15 in monomer 1, and 11-20 and 88-90 in monomer 2, and as such these regions have been excluded from our final model.

BspA-V adopts a fold that is distinct from those reported for other AgI/II family polypeptide V domains (11,12). This consists of two anti-parallel β-sheets, S1 and S2, comprising 5 and 7 strands respectively (Fig 6C). The two sheets are interconnected by four loops and the strands connected by five β-hairpins. There are ten β-bulges in the structure (three G1 bulges, two wide bulges, and five classic β-bulges), of which six occur between strands, and four within β-hairpins. The six inter-strand β-bulges contribute to shaping the long central strands (β4, β5, β11 and β12) of the protein. In its monomeric form, the N- and C-terminal strands of BspA-V (β1 and β12) would converge and be optimally positioned to connect the V domain with its partner A and P domains.

An extended 17 aa residue linker between β1 and β2 projects outward from the surface of the protein exposing a large solvent accessible pocket (~500 $Å^3$, as determined by CASTp (40)) located at the S1-S2 interface (Fig 6C and 6D). The pocket is populated by a combination of hydrophobic and negatively charged residues, consistent with a role in binding carbohydrates or glycoproteins, and is peripherally decorated with polar and negatively charged amino acids. Given the absence of any additional cavities, clefts, or highly charged surfaces, it is likely that this pocket constitutes the ligand binding site of BspA-V domain. The lack of compelling electron density for a number of the residues that constitute the loop linking strands β1 and β2 implies that this region of the protein is flexible, suggesting that it may play a role in gating access to the BspA-V ligand binding pocket (Fig 6C and 6D).

DALI analysis (41) identifies a single functionally analogous structural homologue of BspA-V domain, the carbohydrate binding protein RbmA from *Vibrio cholerae* (42). RbmA is a dimeric protein that promotes biofilm scaffolding via protein-carbohydrate interactions. In contrast to BspA-V, however, carbohydrate binding by RbmA is proposed to occur at either the interface of the RbmA dimer, or within a positively charged ordered loop present in each monomer. Both these structural features are absent in BspA-V implying

that the two proteins employ functionally distinct binding mechanisms.

The BspA-A and -P domains form an anti-parallel coiled-coil super-helix stabilized through an asparagine dependent hydrogen bond network

Having elucidated the molecular structures of the BspA-V and -C domains we next turned our attention to the A and P domains of this protein. A common structural feature of AgI/II family polypeptides is the presence of an extended antiparallel coiled-coil super helix resulting from association of their A and P domains (9). This stalk-like structure serves to project the V domain of the protein away from the bacterial cell surface, where the N and C domains are located, and in previously characterized AgI/II proteins arises due to the complementary "knobs-into-holes" packing of hydrophobic residues within the alanine-rich A domain and PxxP motifs present in the polyproline P domain (9). Bioinformatic analysis of the A and P domains from Bsp proteins demonstrates that these regions are significantly shorter than those of other AgI/II family polypeptides (117-168 residues for Bsp-A domains and 77-102 residues for Bsp-P domains) and differ considerably in amino acid composition. Most notably Bsp-A domains are largely devoid of the AxYxA(LV) heptad motif identified in SpaP and conserved in AspA and SspB (8). In an effort to reconcile these features the A and P domains of BspA were produced recombinantly and their ability to associate *in vitro* examined. Initially circular dichroism (CD) spectroscopy was used to monitor BspA-A/P association and assess changes in helicity resulting from coiled-coil formation. The CD spectrum of BspA-A is consistent with this domain adopting a predominantly α-helical structure, with >55% helicity as predicted using CDSSTR (43-47). BspA-P domain exhibits a CD spectrum consistent with an unfolded protein. Sequential titration of BspA-A into BspA-P, as monitored by CD spectroscopy, demonstrates a stepwise recovery in helicity, consistent with the formation of a coiled-coil structure (Fig 7A). To further characterize the BspA-A/P interaction isothermal titration calorimetry (ITC) was used to monitor the thermodynamic parameters of BspA-A/P formation. Experiments titrating BspA-A into BspA-P were performed (Fig 7B). These analyses demonstrate that the BspA-A/P interaction is predominantly enthalpically driven with ΔG = - 38 ± 4 kJ/mol, K_a= 4.3 ± 0.7 μM^{-1}, K_d = 270 ± 3 nM, ΔH= -660 ± 18 kJ/mol, ΔS = -2.1 kJ/mol/K, and n = 0.62 ± 0.01, at a temperature of 298 K.

Next, we sought to demonstrate that BspA-A/P domain mixing results in the formation of a single, tightly associated A/P complex. To investigate this the hydrodynamic properties of BspA-A, BspA-P and BspA-A/P domains were assessed using SEC (Fig 7C). Comparison of the elution profiles of recombinant BspA-A and BspA-P with those of proteins of known molecular mass (Fig 7D) are consistent with masses of >30 kDa and >20 kDa respectively, significantly larger than those established by SDS-PAGE (Fig 7C). However, given that SEC elution behavior is dictated by Stokes radius rather than molecular mass (48), the elution behavior of BspA-A and BspA-P are consistent with both proteins being single species of extended conformation in solution. A BspA-A/P complex, generated by mixing BspA-A and BspA-P in near-equimolar quantities, yields a single species that elutes prior to both BspA-A and BspA-P domains. SDS-PAGE analysis of this species confirms the presence of both BspA-A and BspA-P domains in this species (Fig 7C). Together our spectroscopic, thermodynamic and hydrodynamic data are fully consistent with the ability of BspA-A and BspA-P domains to self-assemble to form a super-helical structure.

In an effort to investigate the molecular basis of BspA-A/P complex formation a molecular model of this assembly was generated (Fig 7E). Inspection of this model suggests the BspA-A/P helical assembly is mediated largely via an asparagine seam, present on the A domain, which forms a series of complementary hydrogen bond interactions to main chain oxygen and nitrogen atoms within BspA-P domain. The BspA-A/P model remains extended over 200 ns of molecular dynamics simulations (Fig 8). To test the validity of our model an asparagine-less mutant of BspA-A domain was generated (BspA-$A_{\Delta Asn}$) within which all 19 asparagines were substituted to alanines. BspA-$A_{\Delta Asn}$ exhibits a CD spectrum near-identical to that of BspA-A, demonstrating that the helical structure of BspA-$A_{\Delta Asn}$ is not perturbed by the Asp-Ala substitutions (Fig 7F). Titration of BspA-$A_{\Delta Asn}$ into BspA-P, monitored using CD spectroscopy, reveals no increase in helicity. Similarly ITC (data not shown) and SEC analyses

(Fig 7G) provide no evidence of BspA-$A_{\Delta Asn}$/P interaction or complex formation, illustrating the critical role of the BspA-A domain asparagine seam in BspA-A/P assembly.

DISCUSSION

GBS is a leading cause of severe, invasive bacterial infection and represents a significant global health and economic burden (2). Studies of the machineries employed by this bacterium to invade and colonize human hosts are thus of both broad fundamental interest and potential significance for informing the design of new therapeutic agents or interventions. AgI/II family polypeptides are important colonization determinants of oral viridans streptococci and have been identified in GBS (49,50). Our bioinformatic analyses demonstrate that five GBS strains, representing four capsular serotypes, carry genes encoding AgI/II family polypeptides, which we here designate as Bsp proteins. These data support a recent study in which the presence of ICEs carrying a *bsp* gene was shown to be prevalent across a collection of 303 GBS strains derived from 11 host species, including humans, cattle and fish (50). Given the capacity for ICEs to undergo sequence deletions during mobilization, the frequency with which an intact *bsp* gene has been acquired by these strains supports the hypothesis and our findings here that Bsp proteins convey an important competitive advantage to GBS. Analysis of *bsp* gene sequences suggests that they conform to the canonical AgI/II family N-A-V-P-C domain architecture. Nonetheless, the significant sequence variations exhibited by Bsp proteins, as compared to other AgI/II family polypeptides (8), implies a disparity in both domain size and architecture, and hints at a diversification of function.

AgI/II family polypeptides have been shown to play important roles in host colonization by facilitating binding interactions with epithelial cell surfaces (30,51,52). The ability of the archetypal Bsp family member BspA to facilitate binding to vaginal epithelial cells when presented on the surface of non-adherent bacterium *L. lactis* suggests a role for BspA, and perhaps other Bsp proteins, in facilitating host cell adherence and colonization. This has implications for disease risk associated with GBS carriage. Furthermore, a potential target for mucosal tissue colonization is identified as innate immune component gp340. BspA was shown to bind immobilized gp340 via a mechanism that appeared to be dependent upon the BspA-V domain. Vaginal epithelial cells express high levels of cell-associated gp340, and gp340 targeting as a bridging molecule to support epithelial cell interactions has already been shown for HIV (53). Likewise attachment of GBS pili to immobilized gp340 within the oral cavity has been proposed as a potential mechanism to promote GBS colonization of the oropharynx of adults and neonates, an initial step in progression of invasive diseases (25,54). BspA-mediated interactions with immobilized gp340 may therefore represent an important mechanism for facilitating GBS colonization of infection-relevant sites.

AgI/II family polypeptides of oral streptococci have been shown to promote bacterial cell interactions with other resident microbes, a process fundamental to the accretion of oral microbial biofilm communities. Likewise, colonization of the GU tract by the resident microbiota results from the formation of polymicrobial communities on the vaginal epithelium (55). This study provides the first evidence of interkingdom interactions between GBS and *C. albicans*. Given the reported co-isolation of these two species (33-35), candidal-GBS interactions may serve as an important mechanism to promote co-colonization of the GU tract. BspA-expressing *L. lactis* cells were shown to interact with *C. albicans*, binding preferentially to hyphal filaments. AgI/II family polypeptide SspB promotes *S. gordonii* binding to *C. albicans* hyphae via recognition of the hypha-specific adhesin Als3 (24). A similar molecular mechanism may underpin the targeting of BspA to *C. albicans* hyphae.

Our demonstration of the potential role of Bsp proteins in facilitating GBS colonization encouraged us to probe in greater detail the molecular determinants of target recognition by Bsp polypeptides. Although they retain the same general architecture as other AgI/II family proteins, the aa sequences of Bsp proteins suggested functional divergence. Our structural studies provide evidence for a mechanism of target binding that is distinct from other AgI/II family adhesins. The C-terminal domain of BspA lacks a discrete C1 subdomain, proposed to enable the binding of carbohydrates or glycoproteins via the C1-C2 interface. Further, the absence of bound metal ions, suggested in other AgI/II family polypeptide C-

terminal domains to affect stability and adhesive properties (13-16), may indicate altered binding behavior. Although it is not possible to discount metal binding capability entirely based on our crystallographic studies, variations in aa composition within the C2 and C3 metal binding sites are consistent with loss of this function. As Bsp-V domain antibodies block BspA binding to gp340, it appears unlikely that Bsp-C domain makes any significant contribution to mediating this interaction.

Our proposed role of BspA-V domain in target binding is consistent with studies of other AgI/II family polypeptides, where the V domain has been identified as a major determinant of adherence (8). The crystal structure of BspA-V domain demonstrates that this domain adopts a fold that is distinct from those reported for other AgI/II family polypeptides, comprising an elaborated β-sandwich core, which exposes a sizeable binding pocket at the interface of its two constituent β-sheets. The BspA-V domain has no structural precedent amongst AgI/II family proteins, or bacterial adhesins in general. The binding pocket of BspA is formed by a series of hydrophobic and negatively charged residues, consistent with a role in binding carbohydrates or glycosylated proteins. Gp340 is a highly complex molecule designed to recognize many microbial ligands. As such, gp340 contains numerous *N*- and *O*-linked glycosylation sites together with multiple domains (SRCR, CUB) within the protein backbone (56). Given the architecture of BspA-V domain it is likely that gp340 recognition occurs at a site distinct to those targeted by other AgI/II family polypeptides. The role of Bsp proteins as multifunctional adhesins correlates with our findings that BspA targets gp340, vaginal epithelium and *C. albicans*, and is further supported by the recent evidence that BspC may contribute to biofilm formation (50).

Alike to other AgI/II family polypeptides, Bsp proteins retain a coiled-coil super helical A/P domain stalk structure. *In vitro* assembly of the A/P domain complex unambiguously demonstrates that recombinant BspA-A and BspA-P domains self-assemble to form a discrete BspA-A/P species, consistent with an elongated super-helix. However, Bsp proteins lack the defining sequence features observed in SpaP, SspB and AspA (9) that are involved in stabilizing the stalk via hydrophobic interactions. Our modelling studies highlight that the proposed assembly mechanism of SpaP and SspB A/P super-helices is not applicable to BspA. By contrast BspA-A/P assembly is facilitated through a hydrogen bond network primarily contributed to by asparagine residues present in BspA-A domain. The key role of these residues is further evidenced by the inability of an asparagine-less BspA-A domain mutant to associate with BspA-P domain *in vitro*. As a result of shorter A/P stalk length and the absence of the C1 domain, BspA is predicted to be significantly shorter (25-35 nm) than SpaP (>50 nm) (9). AgI/II family polypeptides in oral streptococcal species have been proposed to act as longer distance adhesins, making initial contacts with host surfaces (8). The shorter length of BspA may reflect that in GBS a two-step process occurs, whereby longer appendages carrying adhesins e.g. pili, establish primary host contacts, enabling BspA to make secondary interactions over shorter distances.

In summary this study identifies BspA as an important adhesin of GBS that could play a pivotal role in facilitating host colonization. BspA binds to epithelial cell surfaces and to another opportunistic member of the human microbiota, *C. albicans*. The prototypical Bsp family member, BspA, is shown to possess a novel molecular architecture distinct from other AgI/II family proteins, including a unique functional variable domain with no structural precedent. This divergent structural configuration could be a key to assisting adhesion and survival of GBS in the presence of commensal streptococci or fungi. Moreover the structural and functional information that we describe for BspA can be developed towards designing novel therapeutics, not only against GBS, but also with potential to impact colonization by *C. albicans*. Vaccines or pharmaceuticals that worked efficiently by targeting this conserved antigen specific to GBS might therefore restrict host colonization or control invasive disease by these two opportunistic pathogens.

EXPERIMENTAL PROCEDURES

Bacterial strains and growth conditions

Strains used in this study are outlined in Table 2. *Escherichia coli* K-12 MG1655 was used for molecular cloning experiments to generate pMSP7517-based constructs (abbr. pMSP), Stellar™ competent cells were used to generate pOPINF-based constructs, and *E. coli* BL21(DE3)

was used for expression of recombinant proteins. The methionine auxotroph *E. coli* B834(DE3) was employed for expression of selenomethionine (SeMet) labelled proteins. All *E. coli* strains were cultured in Luria Bertani (LB) medium at 37 °C, with shaking at 220 rpm. *Streptococcus* strains were cultured in Todd-Hewitt broth containing 0.5% yeast extract (THY). All *Streptococcus* strains were grown at 37 °C in an atmosphere of 5% CO_2. *Lactococcus lactis* strains were cultured in M17 broth supplemented with 0.5% glucose (GM17) in a candle jar at 30 °C. Lactococci carrying nisin-inducible pMSP-based constructs were subcultured into GM17 medium containing 10-100 ng/ml nisin. *C. albicans* SC5314 was cultivated on Sabouraud dextrose agar (SAB) at 37 ºC for 48 h. Single colonies were used to inoculate YPD broth (2% yeast extract, 4% mycological peptone, 4% glucose) and cells were cultured at 37 °C with shaking at 220 rpm. Media were supplemented when necessary with 100 µg/ml ampicillin (Amp100) or 300 µg/ml erythromycin (Erm300) for *E. coli*; and 5 µg/ml erythromycin (Erm5) for lactococci.

Generation of L. lactis heterologous expression strains

Primers were designed to amplify locus GBS_RS06095 corresponding to full-length BspA (Table 3). *Nco*I and *Xho*I restriction sites were incorporated at the termini of forward and reverse primers respectively. PCR products were subcloned into nisin-inducible expression vector pMSP (31) via *Nco*I and *Xho*I sites, generating plasmid pMSP.*bspA*$^+$. The construct was transformed directly into electrocompetent *L. lactis* NZ9800, prepared by culturing in GM17G broth (GM17 broth supplemented with 2.5% glycine) at 30 °C to OD_{600nm} 0.5-0.6. Cultures were incubated on ice for 10 min, harvested by centrifugation (3000 *g*, 4 °C, 10 min) and suspended in wash buffer (0.5 M glucose, 10% glycerol). Cells were electroporated in chilled electroporation cuvettes (2 mm electrode gap) using a Bio-Rad Gene Pulser set at 2.5 kV voltage, 25 µF capacitance and 400 Ω resistance. Transformants were recovered in SGM17MC medium (GM17 supplemented with 0.5 M sucrose, 20 mM $MgCl_2$ and 2 mM $CaCl_2$), plated onto GM17 agar supplemented with 5 µg/ml erythromycin and incubated for 48 h at 30 °C in a candle jar. Transformants were confirmed by plasmid isolation and PCR, while expression of BspA in *L. lactis* was verified by dot immunoblot.

Dot immunoblot

Expression of BspA on the surface of *L. lactis* was induced by culturing cells in the presence of 10-100 ng nisin/ml. Suspensions were adjusted to OD_{600nm} 2.0 and spotted (2 µl) onto nitrocellulose membrane. The membrane was blocked with TBS (50 mM Tris-HCl, pH 7.2, 0.15 M NaCl) containing 10% (w/v) milk powder, and subsequently probed with rabbit α-Spy1325mid (25) followed by swine anti-rabbit IgG-horseradish peroxidase (HRP) conjugate (Dako), both diluted 1 in 1000 into TBS supplemented with 0.1% Tween-20 and 1% milk powder. The membrane was then developed using Amersham™ ECL™ Western Blotting Analysis System (GE Healthcare) according to manufacturer's instructions.

In vitro gp340 binding assays

Gp340 was prepared from parotid saliva samples pooled from multiple donors using a multi-step procedure including adsorption onto *S. mutans* cells, as described previously (18). Adherence of *L. lactis* cells expressing BspA to immobilized gp340 was performed by crystal violet assay and data converted to cell numbers as previously described (25).

Antibody inhibition assays

Antibodies reactive against BspA-V (α-rV.BspA) were affinity purified from antibodies raised against AspA (α-Spy1325mid) (25) by a protocol adapted from Jenkinson *et al*., (1990) (57). Nitrocellulose membrane disks (4 cm diameter) were soaked in 250 µl recombinant BspA-V (25 mg/ml) and left to dry for 10 min. Disks were blocked by incubating in TBS containing 10% (w/v) milk (TBSm) for 1 h, then washed with TBS and incubated for 3.5 h with 3.5 ml α-Spy1325mid diluted 1 in 10 in TBSm. Residual antibody was collected for analysis and disks were washed 3 times in TBS. The disks were incubated in 3.5 ml 0.2 M glycine hydrochloride for 8 min at 25 °C and then neutralized with 1 M K_2HPO_4. Dialysis into PBS (50 mM Na_2HPO_4-NaH_2PO_4, pH 7.2, 0.15 M NaCl) was performed by concentrating antibodies with a 10 kDa concentrator (Vivaspin, GE Healthcare). Antibodies were stored at 4 °C. To check antibody specificity, recombinant proteins (see below) corresponding to BspA-V, BspA-P or BspA-C domains (0.6 mg/ml) were two-fold serially diluted and spotted onto nitrocellulose membrane. The blots were probed with antiserum α-Spy1325mid

(1:1000) or affinity purified α-rV.BspA (0.1 mg) and developed as described above.

Coating of microtiter plate wells with gp340 was as described previously (25). Lactococci were harvested (5000 *g*, 7 min), washed in TBSC (TBS containing 5 mM $CaCl_2$), resuspended in 1.5 mM fluorescein isothiocyanate (FITC) in carbonate buffer (50 mM Na_2CO_3, 100 mM NaCl) and incubated for 1 h at 22 ºC in the dark with gentle agitation. Cells were harvested (5000 *g*, 7 min), washed three times in carbonate buffer and suspended in TBSC at OD_{600nm} 1.0. FITC-labelled *L. lactis* cells were incubated with or without 12.5 µg α-rV.BspA for 30 min at 25 °C. Suspensions (50 µl) were transferred to appropriate wells and incubated at 37 °C for 2 h. Wells were washed twice with TBS and fixed by adding 100 µl 25% formaldehyde for 30 min at 25 °C. Formaldehyde was removed and wells were washed twice with TBS before detection of binding levels using a fluorescence plate reader (excitation wavelength 485 nm, emission wavelength 535 nm).

C. albicans binding assays

After 16 h growth in YPD, *C. albicans* cells were harvested (5000 *g*, 5 min), washed and resuspended in YNBPT (20 mM Na_2HPO_4-KH_2PO_4 pH 7.0, 1 x yeast nitrogen base [YNB], 0.02% tryptone) at OD_{600nm} 1.0. Adjusted cell suspensions (200 µl; 2 x 10^5 cells) were transferred to glass bijoux bottles containing 1.8 ml YNBPTG (YNBPT supplemented with 0.4% glucose) and incubated at 37 °C, 220 rpm for 3 h to induce filamentation. Lactococci or GBS cells were harvested (5000 *g*, 7 min), washed in YNBPT, FITC labelled as described above and suspended in YNBPTG at OD_{600nm} 0.2. FITC-labelled bacteria (1 ml; 1 x10^8 cells) were added to each bijoux containing hypha-producing *C. albicans* and incubated at 37 °C, 220 rpm for a further 1 h. Freshly prepared Calcofluor white (1 µg/ml final concentration) was added to each suspension just prior to depositing co-cultures (10 µl) onto microscope slides and visualizing by fluorescence microscopy.

VK2/E6E7 binding assays

Immortalized human vaginal (VK2/E6E7) epithelial cell lines were obtained from American Type Culture Collection (ATCC CRL-2616) and maintained at 37 °C with 5% CO_2 in keratinocyte serum-free medium (KSFM; Gibco®) supplemented with 0.1 ng/ml human recombinant epidermal growth factor, 0.05 mg/ml bovine pituitary extract and 0.4 nM $CaCl_2$. Bacterial association assays were performed as described by Sheen *et al.,* (2011) (5), with minor modifications. In brief, VK2/E6E7 cells (10^5) were seeded into 24-well plates and grown to confluence. Monolayers were then washed and incubated with *L. lactis* suspensions at a MOI of 5 for 2 h at 37 ºC. Nonadherent bacteria were removed by washing, the monolayers were dispersed with trypsin/EDTA (0.1 ml), and then lysed with 0.025% Triton X-100 in water (0.4 ml). Serial dilutions of this lysate were plated onto GM17 agar plates to enumerate associated bacterial colony forming units (CFU).

Protein expression and purification

Primers were designed to amplify regions of locus GBS_RS06095 corresponding to full-length BspA ($BspA_{39-881}$), V domain (BspA-$V_{285-451}$), C-terminal domain (BspA-$C_{554-881}$), A domain (BspA-$A_{117-284}$), and P domain (BspA-$P_{452-553}$), and also a synthetic gene (MWG Eurofins) encoding a variant of the BspA-A domain within which all asparagine residues were substituted to alanine residues (BspA-$A_{\Delta Asn}$) (Table 3). PCR products from amplification of GBS strain NEM316 chromosomal DNA were cloned into the pOPINF expression vector using the In-Fusion™ recombinase (Clontech), incorporating a 6x His-tag at the N-terminus of the cloned product. pOPINF was linearized as described previously (58). pOPINF and PCR amplicons were purified using a Nucleospin PCR Clean-up kit (Clontech) and ligated as instructed by the manufacturer's protocol. All constructs were verified by DNA sequencing. A nucleotide substitution (2231G>A) was identified in *bspA-C*, resulting in a point mutation of Gly_{744} to Asp (G744D). This protein was designated BspA-C_{G744D}. A new construct was subsequently generated lacking this mutation, which was designated BspA-C.

Resulting plasmids were transformed into competent *E. coli* BL21(DE3) cells. Expression strains were grown in 1 L of LB medium to OD_{600nm} 0.4-0.6, at which time IPTG (0.2 mM final concentration for BspA-V and BspA-C; 1 mM for BspA, BspA-A, BspA-$A_{\Delta Asn}$ and BspA-P) was added and the culture incubated at 20 °C, 220 rpm for a further 16 h. Cells were harvested by centrifugation (5000 *g*, 15 min, 4 °C), washed in His-Load buffer (20 mM imidazole, 50 mM Tris, 150 mM NaCl, pH 7.5) and cell pellets frozen at -80 °C.

For SeMet substituted BspA-V, pOPINF-*bspA-V* was transformed into competent *E. coli* B834(DE3) cells. Cells were grown to OD_{600nm} 0.4-0.6, harvested by centrifugation (5000 *g*, 15 min, 4 ºC), washed with distilled water to remove residual methionine and resuspended in 5 ml 50 mM Tris-HCl, pH 7.5. This suspension was then used to inoculate 1 L of pre-warmed M9 medium containing 2.2% (w/v) SeMet Medium Base, 10.2% (w/v) Nutrient Mix and 0.014% (w/v) SeMet (all Molecular Dimensions Ltd.). The culture was grown to OD_{600nm} 0.6, IPTG (0.2 mM final concentration) was added and the culture incubated at 37 ºC with shaking for a further 16 h. Cells were harvested by centrifugation (5000 *g*, 15 min, 4 °C), washed in His-Load buffer supplemented with 1 mM *tris*(2-carboxyethyl)phosphine-HCl (TCEP-HCl, pH 7.5) and the cell pellet frozen at -80 °C.

Frozen cell pellets were resuspended in His-load buffer supplemented with Pierce Protease inhibitor minitablets (Thermo Scientific). Cells were lysed by sonication and cellular debris was removed by centrifugation (20000 *g*, 30 min, 4 °C). Lysates were purified by nickel affinity chromatography using a HiTrap IMAC column (GE Healthcare), followed by size exclusion chromatography (SEC) using either a High Load 16/60 Superdex 75 column (BspA-V, BspA-C; BspA-A, BspA-$A_{\Delta Asn}$, BspA-P), or a Superdex 200 column (BspA) (both GE Healthcare).

Protein crystallization, data collection and processing

BspA-C_{G744D}, BspA-C and SeMet labelled BspA-V were concentrated to 17 mg/ml, 23 mg/ml and 25 mg/ml respectively in buffer comprising 20 mM Tris, 150 mM NaCl, pH 7.5. SeMet labelled BspA-V crystals were grown in 0.1 M Buffer System 1 at pH 6.5 (MES, imidazole), 0.1 M amino acids and 37.5% MPD_P1K_P3350 (Morpheus screen, Molecular Dimensions Ltd). BspA-C_{G744D} crystals were grown in 0.1 M MMT buffer (1:2:2 L-malic acid, MES, Tris-HCl pH 6.0) and 25% (w/v) PEG 1500. BspA-C crystals were grown in 0.02 M sodium/potassium phosphate and 20% (w/v) PEG 3350. X-ray diffraction data were collected on beamlines I03 or I04 at Diamond Light Source, UK. Data for BspA-V and BspA-C were processed with MOSFLM (59). Data for BspA-C_{G744D} were processed with XDS (60). All data collection and refinement statistics are provided in Table 4.

Structure determination

The structure of BspA-V domain was determined using the single wavelength anomalous dispersion method (SAD) as applied to SeMet labelled crystals of BspA-V. Identification of heavy atom sites and the resulting initial phase calculation was carried out using PEHINIX AUTOSOL (61). This was followed by iterative rounds of manual model building and refinement using COOT (62) and REFMAC (63), the latter as implemented in the CCP4 suite of programmes (64). The final model of BspA-V domain comprises two copies of the protein, each encompassing residues 285-451 of the native sequence, 64 water molecules, and 1 molecule each of acetate, diethylene glycol, and ethylene glycol, 96.44% of residues are in allowed or favoured region of the Ramachandran plot with 5 outliers (Lys-295, Asp-325, Val-327, Asp-348, Gln-370).

The structure of BspA-C_{G744D} was determined by molecular replacement using PHASER (65) employing the *S. gordonii* SspB-$C_{1083-1413}$ (13) as a search model (PDB code 2WOY, 33% identity). The initial structure was subjected to iterative rounds of manual model building and refinement using COOT and REFMAC respectively. The final model of BspA-C_{G744D} comprises one copy of the protein and 320 water molecules. 98.50% of residues are in allowed or favoured region of the Ramachandran plot; there were no outliers.

The structure of BspA-C domain was determined by molecular replacement using MOLREP (66) employing BspA-C_{G744D} as a search model. Model building and refinement was performed as detailed above for BspA-C_{G744D}. The final model of BspA-C comprises one copy of the protein, 53 water molecules, 1 molecule of diethylene glycol, and 2 molecules of ethylene glycol, 96.10% of residues are in allowed or favoured region of the Ramachandran plot with one outlier (Asn-743).

Circular dichroism spectroscopy

CD spectra were collected using a Jasco 810 spectropolarimeter (Jasco, Tokyo, Japan) fitted with a Peltier temperature controller. All spectra were collected from 190 to 260 nm, using a 1 mm pathlength cuvette, at 20 °C, in buffer comprising 20 mM sodium phosphate, 50 mM sodium fluoride, pH 7.5. All proteins were dialyzed into this buffer prior to experimentation. Titration experiments were conducted by the sequential addition of BspA-

P in 9.1 µl increments to BspA-A or BspA-$A_{\Delta Asn}$, to a final concentration of 12.3 µM BspA-A and 11.7 µM BspA-P respectively. Final spectra were generated as averages of 8 repeat scans, with appropriate protein-free buffer spectra subtracted. All data were plotted without smoothing using Excel. Spectra were analyzed using the DICHROWEB suite of programmes (46,47). Secondary structure predictions were performed using the CDSSTR method (43-47).

Isothermal titration calorimetry

Calorimetric titrations were performed using a MicroCal iTC200 system (GE Healthcare). The reaction cell (250 µl) contained BspA-A, BspA-$A_{\Delta Asn}$, or BspA-P domains at concentrations ranging from 4 to 12 µM. The syringe (40 µl) contained BspA-A, BspA-$A_{\Delta Asn}$, or BspA-P at concentrations ranging from 48 to 130 µM. Experiments were carried out in reaction buffer comprising 20 mM sodium phosphate, 150 mM sodium chloride, pH 7.5, at 25 °C with a stirring speed of 800 rpm. All proteins were dialyzed into reaction buffer prior to experimentation. An initial injection of 0.4 µl (excluded from data fitting) was followed by 19 injections of 2.0 µl, separated by 180 s intervals. Data were fitted with a single binding site model using Origin software (version 7 with MicroCal ITC analysis module) permitting calculation of the thermodynamic properties ΔG, ΔH, ΔS, K_a and stoichiometries (n) of the binding interactions. The enthalpy of dilution of the various titrants were measured by titration into buffer and found to be insignificant.

Analytical size exclusion chromatography

Analytical SEC was performed using a Superdex 75 10/300 GL column (GE Healthcare) in buffer comprising 20 mM sodium phosphate, 150 mM NaCl, pH 7.5. 200 µl aliquots of each sample (20 µM) were loaded onto the column and eluted at 0.5 ml/min for 30 minutes. The absorbance of the column eluant was monitored at 280 nm throughout.

Molecular modeling

The only template for homology modelling the BspA-A/P domain is the *S. mutans* adhesin SpaP (PDB 3IOX). In this structure the seam between the α-helical (A) and PPII (P) components is formed by stretches of Asn sidechains interacting with the P backbone and stretches of Tyr residues interdigitating P proline sidechains. The BspA-A/P domain is about three times longer than the corresponding region in the 3IOX structure and the A domain is rich in Asn (10%) while poor in Tyr (2%). Mapping the sequence of BspA-A/P domain onto a template derived from 3 copies of the 3IOX A/P domain failed to capture many Asn to P backbone interactions due to supercoiling in the domain. Hence, an alternative approach was sought and an appropriate template was constructed in the following manner: Firstly a regular α-helix was built with the sequence BspA-A A71-N288 and flanked by 2 turns of glycine residues, resulting in a linear seam, comprising the majority of Asn residues, along one face of the helix. Copies of a short, Asn-rich section of the 3IOX A/P domain (A420-K446, P848-V861) were superimposed along the template helix, providing a guide to model the P domain from 3 copies of the 3IOX P domain with minimal adjustments of backbone torsion angles. The P domain sequence D452-T553 was also flanked by glycine residues and 10 registers of this P sequence were threaded onto the template, sidechains repacked with SCWRL (67) and the interaction energy of each thread evaluated with BUDE (68). The best energy model was prepared for energy calculations under the AMBER99-SB-ildn force field using the GROMACS tools to add hydrogen atoms consistent with pH 7, and surrounding the protein in a box of TIP3P waters containing 0.15 M sodium chloride. Molecular dynamics simulations (200 ns) were performed under periodic boundary conditions using PME electrostatics at 278 K and 1 bar as an NTP ensemble. The two components (A and P) were treated in the same way. Setup, simulations and analysis were performed using GROMACS 4.6.7, structure processing and imaging with Chimera 1.9 and VMD 1.9.1.

Statistical analysis

All data are reported as mean ± standard deviation (SD) unless otherwise indicated. Significance between samples was determined using the two-tailed Student's *t*-test, and a value of $P < 0.05$ was accepted as indicating significance. Data were analyzed with GraphPad Prism v6 software.

Acknowledgements: SR was supported by a University of Bristol PhD scholarship. This work was funded in part by BBSRC grant BB/I006478/I (to PRR), NIH grants DE016690 (to HFJ and RJL) and DE012505 (to RJL), and through the award of a Royal Society University Research Fellowship to PRR (UF080534). We thank Jane Brittan and Lindsay Dutton for technical assistance and Catherine Back for advice and discussions. We thank Nicklas Strömberg for provision of gp340, Shaynoor Dramsi for GBS strains and Gary Dunny for plasmid pMSP7517.

Conflict of interest: The authors declare that they have no conflicts of interest with the contents of this article.

Author contributions: HFJ, RJL, PRR and AHN conceived and designed the study. SR, TJH, GRP, MT, AR, RBS, RPR, HFJ, PRR and AHN performed experiments and analysed data. SR, HFJ, RJL, PRR and AHN wrote the manuscript.

REFERENCES

1. Berner, R. (2002) Group B streptococci during pregnancy and infancy. *Curr Opin Infect Dis* **15**, 307-313
2. Le Doare, K., and Heath, P. T. (2013) An overview of global GBS epidemiology. *Vaccine* **31**, D7-12
3. Verani, J. R., McGee, L., and Schrag, S. J. (2010) Prevention of perinatal Group B streptococcal disease-revised guidelines from CDC. *MMWR Rep* **59**, 1-36
4. Baron, M. J., Bolduc, G. R., Goldberg, M. B., Auperin, T. C., and Madoff, L. C. (2004) Alpha C protein of Group B *Streptococcus* binds host cell surface glycosaminoglycan and enters cells by an actin-dependent mechanism. *J Biol Chem* **279**, 24714-24723
5. Sheen, T. R., Jimenez, A., Wang, N. Y., Banerjee, A., van Sorge, N. M., and Doran, K. S. (2011) Serine-rich repeat proteins and pili promote *Streptococcus agalactiae* colonization of the vaginal tract. *J Bacteriol* **193**, 6834-6842
6. Wang, N. Y., Patras, K. A., Seo, H. S., Cavaco, C. K., Rösler, B., Neely, M. N., Sullam, P. M., and Doran, K. S. (2014) Group B streptococcal serine-rich repeat proteins promote interaction with fibrinogen and vaginal colonization. *J Infect Dis* **210**, 982-991
7. Doran, K. S., and Nizet, V. (2004) Molecular pathogenesis of neonatal Group B streptococcal infection: no longer in its infancy. *Mol Microbiol* **54**, 23-31
8. Brady, L. J., Maddocks, S. E., Larson, M. R., Forsgren, N., Persson, K., Deivanayagam, C. C., and Jenkinson, H. F. (2010) The changing faces of *Streptococcus* antigen I/II polypeptide family adhesins. *Mol Microbiol* **77**, 276-286
9. Larson, M. R., Rajashankar, K. R., Patel, M. H., Robinette, R. A., Crowley, P. J., Michalek, S., Brady, L. J., and Deivanayagam, C. (2010) Elongated fibrillar structure of a streptococcal adhesin assembled by the high-affinity association of α- and PPII-helices. *Proc Natl Acad Sci USA* **107**, 5983-5988
10. Heim, K. P., Crowley, P. J., Long, J. R., Kailasan, S., McKenna, R., and Brady, L. J. (2014) An intramolecular lock facilitates folding and stabilizes the tertiary structure of *Streptococcus mutans* adhesin P1. *Proc Natl Acad Sci USA* **111**, 15746-15751
11. Troffer-Charlier, N., Ogier, J., Moras, D., and Cavarelli, J. (2002) Crystal structure of the V-region of *Streptococcus mutans* antigen I/II at 2.4 Å resolution suggests a sugar preformed binding site. *J Mol Biol* **318**, 179-188
12. Forsgren, N., Lamont, R. J., and Persson, K. (2009) Crystal structure of the variable domain of the *Streptococcus gordonii* surface protein SspB. *Protein Sci* **18**, 1896-1905
13. Forsgren, N., Lamont, R. J., and Persson, K. (2010) Two intramolecular isopeptide bonds are identified in the crystal structure of the *Streptococcus gordonii* SspB C-terminal domain. *J Mol Biol* **397**, 740-751

14. Nylander, A., Forsgren, N., and Persson, K. (2011) Structure of the C-terminal domain of the surface antigen SpaP from the caries pathogen *Streptococcus mutans*. *Acta Crystallogr Sect F: Struct Biol Cryst Commun* **67**, 23-26
15. Larson, M. R., Rajashankar, K. R., Crowley, P. J., Kelly, C., Mitchell, T. J., Brady, L. J., and Deivanayagam, C. (2011) Crystal structure of the C-terminal region of *Streptococcus mutans* antigen I/II and characterization of salivary agglutinin adherence domains. *J Biol Chem* **286**, 21657-21666
16. Hall, M., Nylander, S., Jenkinson, H. F., and Persson, K. (2014) Structure of the C-terminal domain of AspA (antigen I/II-family) protein from *Streptococcus pyogenes*. *FEBS Open Bio* **4**, 283-289
17. Madsen, J., Mollenhauer, J., and Holmskov, U. (2010) Review: Gp-340/DMBT1 in mucosal innate immunity. *Innate Immun* **16**, 160-167
18. Loimaranta, V., Jakubovics, N. S., Hytonen, J., Finne, J., Jenkinson, H. F., and Stromberg, N. (2005) Fluid- or surface-phase human salivary scavenger protein gp340 exposes different bacterial recognition properties. *Infect Immun* **73**, 2245-2252
19. Egland, P. G., Du, L. D., and Kolenbrander, P. E. (2001) Identification of independent *Streptococcus gordonii* SspA and SspB functions in coaggregation with *Actinomyces naeslundii*. *Infect Immun* **69**, 7512-7516
20. Jakubovics, N. S., Stromberg, N., van Dolleweerd, C. J., Kelly, C. G., and Jenkinson, H. F. (2005) Differential binding specificities of oral streptococcal antigen I/II family adhesins for human or bacterial ligands. *Mol Microbiol* **55**, 1591-1605
21. Back, C. R., Douglas, S. K., Emerson, J. E., Nobbs, A. H., and Jenkinson, H. F. (2015) *Streptococcus gordonii* DL1 adhesin SspB V-region mediates coaggregation via receptor polysaccharide of *Actinomyces oris* T14V. *Mol Oral Microbiol* **30**, 411-424
22. Lamont, R. J., El-Sabaeny, A., Park, Y., Cook, G. S., Costerton, J. W., and Demuth, D. R. (2002) Role of the *Streptococcus gordonii* SspB protein in the development of *Porphyromonas gingivalis* biofilms on streptococcal substrates. *Microbiology* **148**, 1627-1636
23. Park, Y., Simionato, M. R., Sekiya, K., Murakami, Y., James, D., Chen, W., Hackett, M., Yoshimura, F., Demuth, D. R., and Lamont, R. J. (2005) Short fimbriae of *Porphyromonas gingivalis* and their role in coadhesion with *Streptococcus gordonii*. *Infect Immun* **73**, 3983-3989
24. Silverman, R. J., Nobbs, A. H., Vickerman, M. M., Barbour, M. E., and Jenkinson, H. F. (2010) Interaction of *Candida albicans* cell wall Als3 protein with *Streptococcus gordonii* SspB adhesin promotes development of mixed-species communities. *Infect Immun* **78**, 4644-4652
25. Maddocks, S. E., Wright, C. J., Nobbs, A. H., Brittan, J. L., Franklin, L., Strömberg, N., Kadioglu, A., Jepson, M. A., and Jenkinson, H. F. (2011) *Streptococcus pyogenes* antigen I/II-family polypeptide AspA shows differential ligand-binding properties and mediates biofilm formation. *Mol Microbiol* **81**, 1034-1049
26. Green, N. M., Zhang, S., Porcella, S. F., Nagiec, M. J., Barbian, K. D., Beres, S. B., LeFebvre, R. B., and Musser, J. M. (2005) Genome sequence of a serotype M28 strain of Group A *Streptococcus*: potential new insights into puerperal sepsis and bacterial disease specificity. *J Infect Dis* **192**, 760-770
27. Brochet, M., Couve, E., Glaser, P., Guedon, G., and Payot, S. (2008) Integrative conjugative elements and related elements are major contributors to the genome diversity of *Streptococcus agalactiae*. *J Bacteriol* **190**, 6913-6917
28. Zhang, S., Green, N. M., Sitkiewicz, I., Lefebvre, R. B., and Musser, J. M. (2006) Identification and characterization of an antigen I/II family protein produced by Group A *Streptococcus*. *Infect Immun* **74**, 4200-4213
29. Sitkiewicz, I., Green, N. M., Guo, N., Mereghetti, L., and Musser, J. M. (2011) Lateral gene transfer of streptococcal ICE element RD2 (region of difference 2) encoding secreted proteins. *BMC Microbiol* **11**, 65

30. Franklin, L., Nobbs, A. H., Bricio-Moreno, L., Wright, C. J., Maddocks, S. E., Sahota, J. S., Ralph, J., O'Connor, M., Jenkinson, H. F., and Kadioglu, A. (2013) The AgI/II family adhesin AspA is required for respiratory infection by *Streptococcus pyogenes*. *PLoS One* **8**, e62433
31. Hirt, H., Erlandsen, S. L., and Dunny, G. M. (2000) Heterologous inducible expression of *Enterococcus faecalis* pCF10 aggregation substance *asc10* in *Lactococcus lactis* and *Streptococcus gordonii* contributes to cell hydrophobicity and adhesion to fibrin. *J Bacteriol* **182**, 2299-2306
32. Purushotham, S., and Deivanayagam, C. (2014) The calcium-induced conformation and glycosylation of scavenger-rich cysteine repeat (SRCR) domains of glycoprotein 340 influence the high affinity interaction with antigen I/II homologs. *J Biol Chem* **289**, 21877-21887
33. Monif, G. R., and Carson, H. J. (1998) Female genital tract bacterial coisolates with *Candida albicans* in patients without clinical vaginitis. *Infect Dis Obstet Gynecol* **6**, 52-56
34. Bayó, M., Berlanga, M., and Agut, M. (2002) Vaginal microbiota in healthy pregnant women and prenatal screening of Group B streptococci (GBS). *Int Microbiol* **5**, 87-90
35. Cools, P., Jespers, V., Hardy, L., Crucitti, T., Delany-Moretlwe, S., Mwaura, M., Ndayisaba, G. F., van de Wijgert, J. H., and Vaneechoutte, M. (2016) A multi-country cross-sectional study of vaginal carriage of Group B streptococci (GBS) and *Escherichia coli* in resource-poor settings: prevalences and risk factors. *PLoS One* **11**, e0148052
36. Jenkinson, H. F., Lala, H. C., and Shepherd, M. G. (1990) Coaggregation of *Streptococcus sanguis* and other streptococci with *Candida albicans*. *Infect Immun* **58**, 1429-1436
37. Kolenbrander, P. E., Ganeshkumar, N., Cassels, F. J., and Hughes, C. V. (1993) Coaggregation: specific adherence among human oral plaque bacteria. *FASEB J* **7**, 406-413
38. Bamford, C. V., d'Mello, A., Nobbs, A. H., Dutton, L. C., Vickerman, M. M., and Jenkinson, H. F. (2009) *Streptococcus gordonii* modulates *Candida albicans* biofilm formation through intergeneric communication. *Infect Immun* **77**, 3696-3704
39. Kelly, C. G., and Younson, J. S. (2000) Anti-adhesive strategies in the prevention of infectious disease at mucosal surfaces. *Expert Opin Investig Drugs* **9**, 1711-1721
40. Dundas, J., Ouyang, Z., Tseng, J., Binkowski, A., Turpaz, Y., and Liang, J. (2006) CASTp: computed atlas of surface topography of proteins with structural and topographical mapping of functionally annotated residues. *Nucleic Acids Res* **34**, W116-118
41. Holm, L., and Rosenstrom, P. (2010) Dali server: conservation mapping in 3D. *Nucleic Acids Res* **38**, W545-549
42. Giglio, K. M., Fong, J. C., Yildiz, F. H., and Sondermann, H. (2013) Structural basis for biofilm formation via the *Vibrio cholerae* matrix protein RbmA. *J Bacteriol* **195**, 3277-3286
43. Compton, L. A., and Johnson, W. C., Jr. (1986) Analysis of protein circular dichroism spectra for secondary structure using a simple matrix multiplication. *Anal Biochem* **155**, 155-167
44. Manavalan, P., and Johnson, W. C., Jr. (1987) Variable selection method improves the prediction of protein secondary structure from circular dichroism spectra. *Anal Biochem* **167**, 76-85
45. Sreerama, N., and Woody, R. W. (2000) Estimation of protein secondary structure from circular dichroism spectra: comparison of CONTIN, SELCON, and CDSSTR methods with an expanded reference set. *Anal Biochem* **287**, 252-260
46. Whitmore, L., and Wallace, B. A. (2004) DICHROWEB, an online server for protein secondary structure analyses from circular dichroism spectroscopic data. *Nucleic Acids Res* **32**, W668-673
47. Whitmore, L., and Wallace, B. A. (2008) Protein secondary structure analyses from circular dichroism spectroscopy: methods and reference databases. *Biopolymers* **89**, 392-400
48. Siegel, L. M., and Monty, K. J. (1966) Determination of molecular weights and frictional ratios of proteins in impure systems by use of gel filtration and density gradient centrifugation. Application to crude preparations of sulfite and hydroxylamine reductases. *Biochim Biophys Acta* **112**, 346-362
49. Tettelin, H., Masignani, V., Cieslewicz, M. J., Donati, C., Medini, D., Ward, N. L., Angiuoli, S. V., Crabtree, J., Jones, A. L., Durkin, A. S., Deboy, R. T., Davidsen, T. M., Mora, M., Scarselli, M., Margarit y Ros, I., Peterson, J. D., Hauser, C. R., Sundaram, J. P., Nelson, W. C., Madupu, R., Brinkac, L. M., Dodson, R. J., Rosovitz, M. J., Sullivan, S. A., Daugherty, S. C., Haft, D. H.,

Selengut, J., Gwinn, M. L., Zhou, L., Zafar, N., Khouri, H., Radune, D., Dimitrov, G., Watkins, K., O'Connor, K. J., Smith, S., Utterback, T. R., White, O., Rubens, C. E., Grandi, G., Madoff, L. C., Kasper, D. L., Telford, J. L., Wessels, M. R., Rappuoli, R., and Fraser, C. M. (2005) Genome analysis of multiple pathogenic isolates of *Streptococcus agalactiae*: implications for the microbial "pan-genome". *Proc Natl Acad Sci USA* **102**, 13950-13955

50. Chuzeville, S., Dramsi, S., Madec, J. Y., Haenni, M., and Payot, S. (2015) Antigen I/II encoded by integrative and conjugative elements of *Streptococcus agalactiae* and role in biofilm formation. *Microb Pathog* **88**, 1-9
51. Al-Okla, S., Chatenay-Rivauday, C., Klein, J. P., and Wachsmann, D. (1999) Involvement of α5β1 integrins in interleukin 8 production induced by oral viridans streptococcal protein I/IIf in cultured endothelial cells. *Cell Microbiol* **1**, 157-168
52. Nobbs, A. H., Shearer, B. H., Drobni, M., Jepson, M. A., and Jenkinson, H. F. (2007) Adherence and internalization of *Streptococcus gordonii* by epithelial cells involves β1 integrin recognition by SspA and SspB (antigen I/II family) polypeptides. *Cell Microbiol* **9**, 65-83
53. Stoddard, E., Cannon, G., Ni, H., Kariko, K., Capodici, J., Malamud, D., and Weissman, D. (2007) gp340 expressed on human genital epithelia binds HIV-1 envelope protein and facilitates viral transmission. *J Immunol* **179**, 3126-3132
54. Brittan, J. L., and Nobbs, A. H. (2015) Group B *Streptococcus* pili mediate adherence to salivary glycoproteins. *Microbes Infect* **17**, 360-368
55. Verstraelen, H., and Swidsinski, A. (2013) The biofilm in bacterial vaginosis: implications for epidemiology, diagnosis and treatment. *Curr Opin Infect Dis* **26**, 86-89
56. Ligtenberg, A. J., Veerman, E. C., Nieuw Amerongen, A. V., and Mollenhauer, J. (2007) Salivary agglutinin/glycoprotein-340/DMBT1: a single molecule with variable composition and with different functions in infection, inflammation and cancer. *Biol Chem* **388**, 1275-1289
57. Jenkinson, H. F., and Easingwood, R. A. (1990) Insertional inactivation of the gene encoding a 76-kilodalton cell surface polypeptide in *Streptococcus gordonii* Challis has a pleiotropic effect on cell surface composition and properties. *Infect Immun* **58**, 3689-3697
58. Berrow, N. S., Alderton, D., Sainsbury, S., Nettleship, J., Assenberg, R., Rahman, N., Stuart, D. I., and Owens, R. J. (2007) A versatile ligation-independent cloning method suitable for high-throughput expression screening applications. *Nucleic Acids Res* **35**, e45
59. Battye, T. G. G., Kontogiannis, L., Johnson, O., Powell, H. R., and Leslie, A. G. W. (2011) iMOSFLM: a new graphical interface for diffraction-image processing with MOSFLM. *Acta Crystallogr D Biol Crystallogr* **67**, 271-281
60. Kabsch, W. (2010) XDS. *Acta Crystallogr D Biol Crystallogr* **66**, 125-132
61. Adams, P. D., Grosse-Kunstleve, R. W., Hung, L. W., Ioerger, T. R., McCoy, A. J., Moriarty, N. W., Read, R. J., Sacchettini, J. C., Sauter, N. K., and Terwilliger, T. C. (2002) PHENIX: building new software for automated crystallographic structure determination. *Acta Crystallogr Sect D: Biol Crystallogr* **58**, 1948-1954
62. Emsley, P., and Cowtan, K. (2004) Coot: model-building tools for molecular graphics. *Acta Crystallogr D Biol Crystallogr* **60**, 2126-2132
63. Murshudov, G. N., Skubák, P., Lebedev, A. A., Pannu, N. S., Steiner, R. A., Nicholls, R. A., Winn, M. D., Long, F., and Vagin, A. A. (2011) REFMAC5 for the refinement of macromolecular crystal structures. *Acta Crystallogr D Biol Crystallogr* **67**, 355-367
64. Winn, M. D., Ballard, C. C., Cowtan, K. D., Dodson, E. J., Emsley, P., Evans, P. R., Keegan, R. M., Krissinel, E. B., Leslie, A. G. W., McCoy, A., McNicholas, S. J., Murshudov, G. N., Pannu, N. S., Potterton, E. A., Powell, H. R., Read, R. J., Vagin, A., and Wilson, K. S. (2011) Overview of the CCP4 suite and current developments. *Acta Crystallogr D Biol Crystallogr* **67**, 235-242
65. McCoy, A. J., Grosse-Kunstleve, R. W., Adams, P. D., Winn, M. D., Storoni, L. C., and Read, R. J. (2007) Phaser crystallographic software. *J Appl Crystallogr* **40**, 658-674
66. Vagin, A., and Teplyakov, A. (2010) Molecular replacement with MOLREP. *Acta Crystallogr D Biol Crystallogr* **66**, 22-25

67. Krivov, G. G., Shapovalov, M. V., and Dunbrack, R. L., Jr. (2009) Improved prediction of protein side-chain conformations with SCWRL4. *Proteins* **77**, 778-795
68. McIntosh-Smith, S., Price, J., Sessions, R. B., and Ibarra, A. A. (2014) High performance *in silico* virtual drug screening on many-core processors. *Int J High Perform Comput Appl* **29**, 119-134
69. Baker, N. A., Sept, D., Joseph, S., Holst, M. J., and McCammon, J. A. (2001) Electrostatics of nanosystems: application to microtubules and the ribosome. *Proc Natl Acad Sci U S A* **98**, 10037-10041
70. Gillum, A. M., Tsay, E. Y., and Kirsch, D. R. (1984) Isolation of the *Candida albicans* gene for orotidine-5'-phosphate decarboxylase by complementation of *S. cerevisiae ura3* and *E. coli pyrF* mutations. *MMG* **198**, 179-182

FOOTNOTES

The content is solely the responsibility of the authors and does not necessarily represent the official views of the NIH.

The atomic coordinates and structure factors of BspA-V, BspA-C_{G744D} and BspA-C have been deposited in the Protein Data Bank under accession codes 5DZ8, 5DZ9, 5DZA respectively.

The abbreviations used are: GBS, Group B *Streptococcus*; GAS, Group A *Streptococcus*; ECM, extracellular matrix; Bsp, Group B *Streptococcus* surface protein; AspA, Group A *Streptococcus* surface protein; PPII, polyproline II; gp340, glycoprotein-340; RD2, region of difference 2; ICE, integrative conjugative element; SEC, size exclusion chromatography; SeMet, selenomethionine, RMSD, root-mean-square deviation; SAD, single anomalous dispersion; ITC, isothermal titration calorimetry.

FIGURE LEGENDS

FIGURE 1. (A) Model structure of Bsp family proteins based on the proposed domain organisation of other AgI/II polypeptides (8,9). This comprises a stalk consisting of the α-helical A domain and the polyproline II (PPII) helical P domain, separating the V domain and the C-terminal domains. The C-terminal domain is followed by the LPxTG motif required for cell wall anchorage. (B) Amino sequence alignment of BspA, BspB, BspC and BspD. Structural regions are colored as in (A) with amino acids conserved in all four proteins highlighted in black.

FIGURE 2. Interactions of BspA with immobilized gp340. (A) Dot immunoblot to verify the expression of BspA on the surface of *L. lactis* NZ9800. Lactococci were cultured for 16 h in the absence (uninduced) or presence of 10 ng/ml or 100 ng/ml nisin to induce BspA expression. Lactococcal suspensions (OD_{600nm} 2.0) were serially two-fold diluted and spotted onto nitrocellulose membrane. The blot was probed with α-Spy1325 mid antibodies to the V region of AspA (25). (B) Binding of *L. lactis* pMSP.*bspA*$^+$ or vector control (pMSP) to immobilized gp340. Induced or uninduced cells were then incubated in microwells coated with 50 ng gp340 (black column) or blocking agent BSA (grey column) for 2 h at 37 °C. Nonadherent cells were removed, and total biomass was measured by crystal violet staining. Values given represent mean ± SD of three independent experiments performed in triplicate.*$P < 0.005$ relative to vector control, calculated using an unpaired Student's *t*-test.

FIGURE 3. Antibody inhibition binding studies. (A) Affinity purification of α-rV.BspA antibodies. Antibodies reactive against recombinant BspA-V (α-rV.BspA) were affinity purified from antibodies raised against AspA (α-Spy1325mid). Purified α-rV.BspA antibodies were used to probe dot immunoblots of serially diluted (1:2) recombinant proteins corresponding to BspA-V, P and C domains. Purified antibodies reacted only with BspA-rV. (B) Effects of affinity-purified antibody α-rV.BspA on adherence of *L. lactis* expressing BspA to immobilized gp340. *L. lactis* pMSP.*bspA*$^+$ cells were FITC-labelled, preincubated without antibody or with 2.4 µg α-rV.BspA, and then incubated in microwells coated with 50 ng gp340 for 2 h at 37 °C. Nonadherent cells were removed, and relative numbers of attached cells measured in a fluorescence plate reader. *L. lactis* pKS80.*sspB*$^+$ expressing *S. gordonii* SspB was included as a control. Values given represent mean ± SD of two independent experiments performed in duplicate. *$P < 0.0001$ relative to no antiserum (A/S) control, calculated using an unpaired Student's *t*-test.

FIGURE 4. Interactions of GBS or lactococci expressing BspA with *C. albicans*. (A) GBS NEM316 cells, (B) *L. lactis* pMSP vector control or (C) *L. lactis* pMSP.*bspA*$^+$. *L. lactis* strains were cultured for 16 h in the absence (uninduced) or presence of 100 ng/ml nisin to induce BspA expression. GBS or *L. lactis* cells were FITC-labelled and incubated in suspension with hypha-forming cells of *C. albicans* stained with Calcofluor white. Aggregates were visualized by fluorescence microscopy. Scale bars, 20 µm.

FIGURE 5. Interactions of *L. lactis* pMSP.*bspA*$^+$ or pMSP vector control with VK2/E6E7 vaginal epithelial cell line. Lactococci (MOI 5) were incubated with monolayers of VK2/E6E7 cells and numbers of associated CFU enumerated from serial dilutions of recovered cell lysates. Values given represent mean ± SD of four independent experiments performed in triplicate.*$P < 0.05$ relative to vector control, calculated using a paired Student's *t*-test.

FIGURE 6. Crystal structures of BspA-V and -C domains. (A) Superposition of the crystal structures of BspA-C_{G744D} (green) and BspC (blue). The location of the two isopeptide bonds are highlighted. (B) Crystal structure of the BspA-V strand-swapped homodimer. (C) Crystal structure of a BspA-V monomer. The domain adopts a β-sandwich fold, consisting of two anti-parallel sheets made-up of five and seven strands respectively. The N- and C-terminal strands meet to connect the V domain with A and P domains respectively. A close up view of the BspA-V target binding pocket is provided as an inset. The putative gating loop is labelled. For clarity, residues within the gating loop for which compelling electron density

was not observed (Asp298 and Asn299) have been excluded from the structure. (D) Electrostatic surface representation of BspA-V mirroring the views of the protein shown in (C). Electrostatic potentials were calculated using APBS (69).

FIGURE 7. Biophysical characterisation of BspA-A/P complex formation. (A) CD spectroscopy of BspA-A, BspA-P, and an equimolar mixture of both proteins. (B) ITC analysis monitoring the titration of BspA-A into BspA-P. (C) SEC elution profiles of BspA-A, BspA-P and the BspA-A/P complex. (D) SEC column calibration curve calculated using Bio-Rad protein standards (thyroglobulin, 670 kDa; γ -globulin, 158 kDa; ovalbumin, 44 kDa; myoglobin, 17 kDa; vitamin B_{12}, 1.35 kDa). (E) Molecular model of the BspA-A/P complex highlighting the role of BspA-A domain (blue) asparagine residues in mediating interaction with BspA-P (green). (F) CD spectroscopy of BspA-$A_{\Delta Asn}$, BspA-P, and an equimolar mixture of both proteins. (G) SEC elution profiles of BspA-$A_{\Delta Asn}$, BspA-P and an equimolar mixture of both proteins.

FIGURE 8. Molecular dynamics simulations of the model of BspA-P/A, BspA-A and BspA-P. (A) Structures at time points during the simulations. The dimeric BspA-P/A model behaves as a semi-rigid rod during the simulation while the BspA-A α-helix shows kinking and partial unfolding of the helix. The PPII BspA-P rapidly collapses into a random coil. Ribbons are rainbow coloured blue N-terminal through red C-terminal. (B) Initial model. The alignment of most of the asparagine residues in BspA-A towards the backbone of BspA-P. Asn residues, pink spheres; Pro residues, magenta spheres. (C) Plots of radius of gyration with respect to time. BspA-A/P, red; BspA-A, green; BspA-P, blue.

TABLE 1. Distribution of AgI/II family polypeptides in GBS

AgI/II gene	Strain (serotype)	Previous locus tag	New locus tag
bspA	NEM316 (III)	gbs1143	GBS_RS06095
bspB	NEM316 (III)	gbs0393	GBS_RS02350
		gbs0723	GBS_RS04015
		gbs0986	GBS_RS05325
bspC	515 (Ia)	SAL_2056	SAL_RS04265
	COH1 (III)	SAN_2127	GBSCOH1_1801
bspD	2603V/R (V)	SAG_2021	-
	18RS21 (II)	SAJ_1924	-

TABLE 2. Microbial strains used in study

Strain		Characteristics	Source
S. agalactiae	NEM316	Wild-type (serotype III)	Laboratory stock
L. lactis	NZ9800	Wild-type	Laboratory stock
	UB2658	pMSP.*bspA*$^{+}$	This study
	UB2635	Empty pMSP	This study
C. albicans	SC5314	Wild-type	Gillum *et al.*, 1984 (70)
E. coli	K-12 MG1655	*F*$^{-}$ *λ*$^{-}$ *rph-1*	Laboratory stock
	Stellar™	*F' endA1 supE44 thi-1 recA1 relA1 gyrA96 phoA Φ80d lacZΔ M15 Δ(lacZYA-argF) U169 Δ(mrr-hsdRMS-mcrBC) ΔmcrA, λ*$^{-}$	Clontech
	B834(DE3)	F^{-} *ompT hsdS*$_B$(r_B^- m_B^-) *gal dcm met* (DE3)	Novagen
	BL21(DE3)	F^{-} *ompT hsdS*$_B$(r_B^- m_B^-) *gal dcm* (DE3)	Novagen
	UB2878	pOPINF.*bspA*$^{+}$; full-length; BL21	This study
	UB2879	pOPINF.*bspA-V*$^{+}$*;* BL21	This study
	UB2880	pOPINF.*bspA-C*$^{+}$; 2231G>A; BL21	This study
	UB2881	pOPINF.*bspA-C*$^{+}$; BL21	This study
	UB2882	pOPINF.*bspA-A*$^{+}$; BL21	This study
	UB2883	pOPINF.*bspA-*$A_{\Delta Asn}$$^{+}$; BL21	This study
	UB2884	pOPINF.*bspA-P*$^{+}$; BL21	This study

TABLE 3. Primers used in study

Protein Product	Primer Name	Sequence[a]
$BspA_{1-932}$	pMSP.*bspA*.F	CATGCCATGGAGGAGGAAACAATATGAATTCAC
	pMSP.*bspA*.R	CCGCTCGAGGCAACCCGATTATGAGAGG
$BspA_{39-881}$	*bspA*-N.F	**AAGTTCTGTTTCAGGGCCCG**GCTGATCAAGTTAC AACTCAAGCA
	bspA-C.R	**ATGGTCTAGAAAGCTTTACTA**TTGCTCTCCTGTG GATGGTAA
$BspA\text{-}V_{285-451}$	*bspA*-V.F	**AAGTTCTGTTTCAGGGCCCG**AATGTTGCTTTTGA CATTAAAGCC
	bspA-V.R	**ATGGTCTAGAAAGCTTTACTA**ATTATTATTAACA TAAGACACTAAAGC
$BspA\text{-}C_{554-881}$	*bspA*-C.F	**AAGTTCTGTTTCAGGGCCCG**CCAACTAAGAAAG TTCTAGATGAA
	bspA-C.R	**ATGGTCTAGAAAGCTTTACTA**TTGCTCTCCTGTG GATGGTAA
$BspA\text{-}A_{117-284}$	*bspA*-A.F	**AAGTTCTGTTTCAGGGCCCG**ATTAAAGATGCTAC TGCTGAAAAT
	bspA-A.R	**ATGGTCTAGAAAGTCTTACTA**ATTAATAGACTGT TTATCTGCTTC
$BspA\text{-}P_{452-553}$	*bspP*-A.F	**AAGTTCTGTTTCAGGGCCCG**GATGCTGTTCCTAA TGTGGTC
	bspP-A.R	**ATGGTCTAGAAAGCTTTACTA**TGTGGCCTTTGGT ATCTGTAC
$BspA\text{-}A_{\Delta Asn}$	*bspA*-$A_{\Delta N}$-F	**AAGTTCTGTTTCAGGGCCCG**ATGGCGAAGAAAG CGGCT
	bspA-$A_{\Delta N}$-R	**ATGGTCTAGAAAGCTTTATCA**GGCAATCGACTGT TTATCGGCTTC

[a]Restriction endonuclease sites are underlined. Sequences in bold indicate additional bases required for cloning into the ligation-independent expression vector pOPINF.

TABLE 4. Crystallization, data collection and refinement statistics

	BspA-$V_{Se\text{-}Met}$	BspA-C_{G744D}	BspA-C_{WT}
PDB IDs	5DZ8	5DZ9	5DZA
Data collection			
Space group	*C*121	$P2_12_12_1$	$C222_1$
Cell dimensions			
a, *b*, *c* (Å)	148.1, 34.4, 92.6	38.1, 48.2, 234.1	34.1, 206.2, 121.4
α, β, γ (°)	90.0, 127.3, 90.0	90.0, 90.0, 90.0	90.0, 90.0, 90.0
Wavelength Å	0.979	0.979	0.920
Resolution range (Å)[a]	73.7-2.4 (2.5-2.4)	58.5-1.9 (1.9-1.8)	39.1-2.2 (2.3-2.2)
R_{merge}	0.06 (0.14)	0.11 (0.84)	0.09 (0.45)
$I / \sigma I$	19.9 (8.6)	17.2 (3.4)	9.7 (1.9)
$CC_{1/2}$ (%)	99.8 (98.8)	99.7 (78.6)	99.6 (76.4)
Completeness (%)	99.6 (97.2)	99.4 (96.4)	92.3 (94.3)
Redundancy	5.9 (4.8)	12.3 (9.9)	3.4 (3.5)
No. of Se sites	4		
FOM	0.25		
Refinement			
Resolution (Å)	73.7-2.4	55.5-1.9	102.9-2.2
No. reflections (working set/test set)	87362/13981	436280/33734	69391/19496
R_{work} / R_{free}	23.5/26.2	19.6/23.4	21.8/23.9
No. atoms	2566	2944	2505
Protein	2487	2624	2437
Ligand/ion	15	0	15
Water	64	320	53
B-factors Å^2			
Protein	25	22	24
Ligand	30		31
Water	29	32	24
R.M.S. deviations			
Bond lengths (Å)	0.02	0.02	0.02
Bond angles (°)	1.7	1.8	1.8

[a]Values in parentheses are for highest resolution shell.

FIGURE 1.

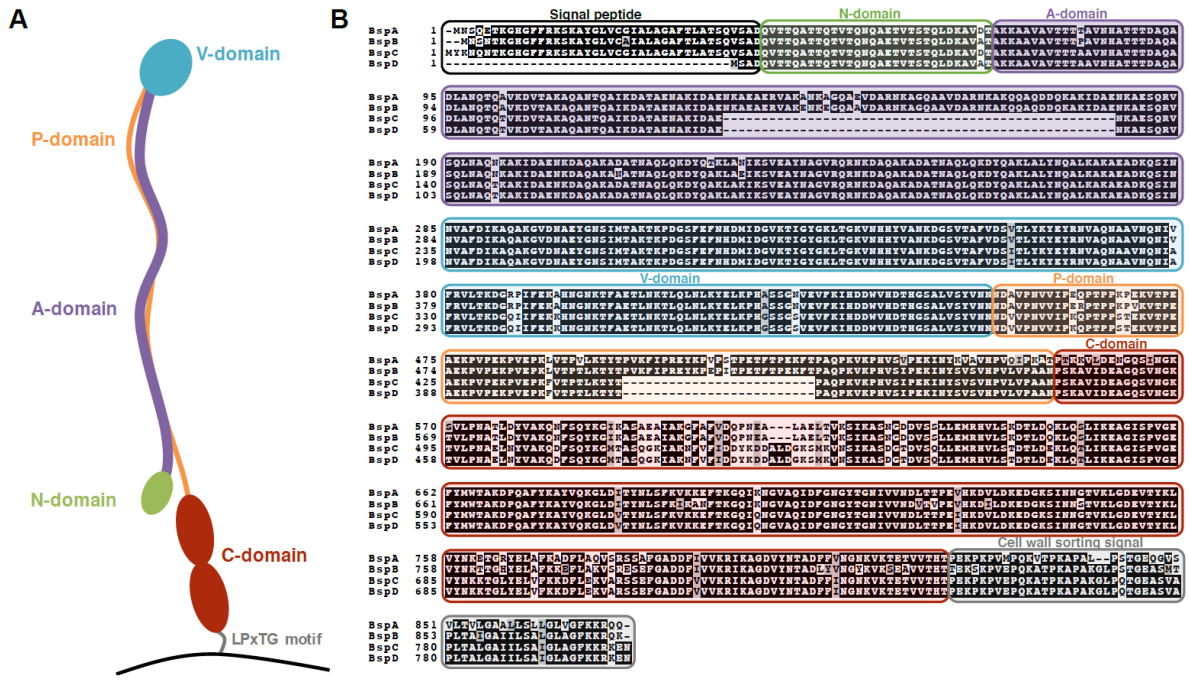
A
V-domain
P-domain
A-domain
N-domain
C-domain
LPxTG motif
B
Signal peptide
N-domain
A-domain
V-domain
P-domain
C-domain
Cell wall sorting signal
BspA
BspB
BspC
BspD

FIGURE 2.

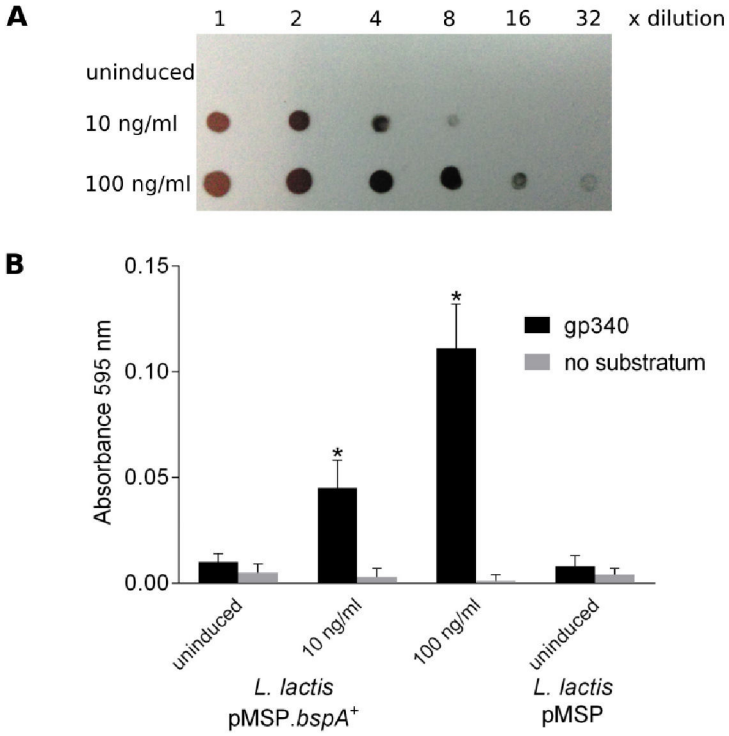
A
1
2
4
8
16
32
x dilution
uninduced
10 ng/ml
100 ng/ml
B
0.15
0.10
0.05
0.00
Absorbance 595 nm
gp340
no substratum
*
*
uninduced
10 ng/ml
100 ng/ml
uninduced
L. lactis
pMSP.bspA+
L. lactis
pMSP

FIGURE 3.

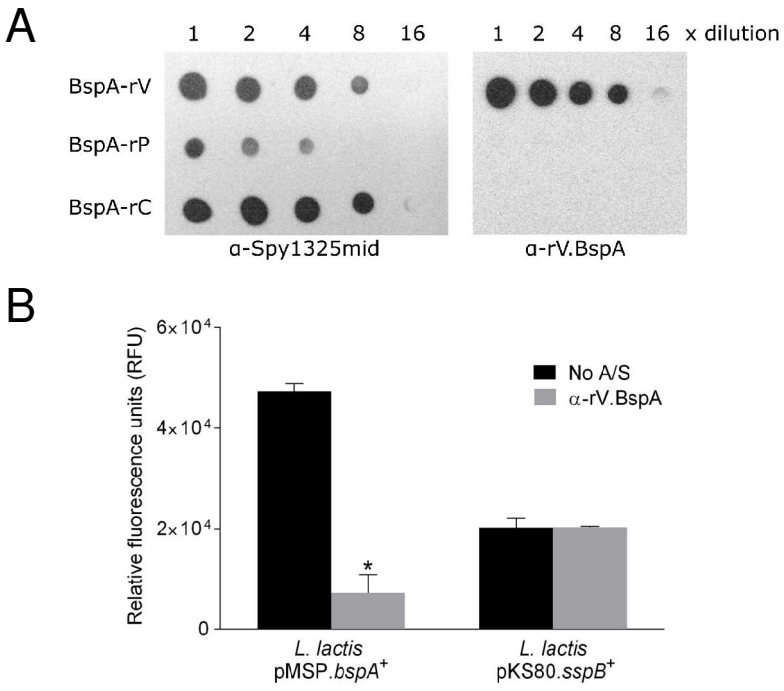
A
1 2 4 8 16
1 2 4 8 16 x dilution
BspA-rV
BspA-rP
BspA-rC
α-Spy1325mid
α-rV.BspA
B
Relative fluorescence units (RFU)
6x10⁴
4x10⁴
2x10⁴
0
No A/S
α-rV.BspA
*
L. lactis pMSP.bspA+
L. lactis pKS80.sspB+

FIGURE 4.

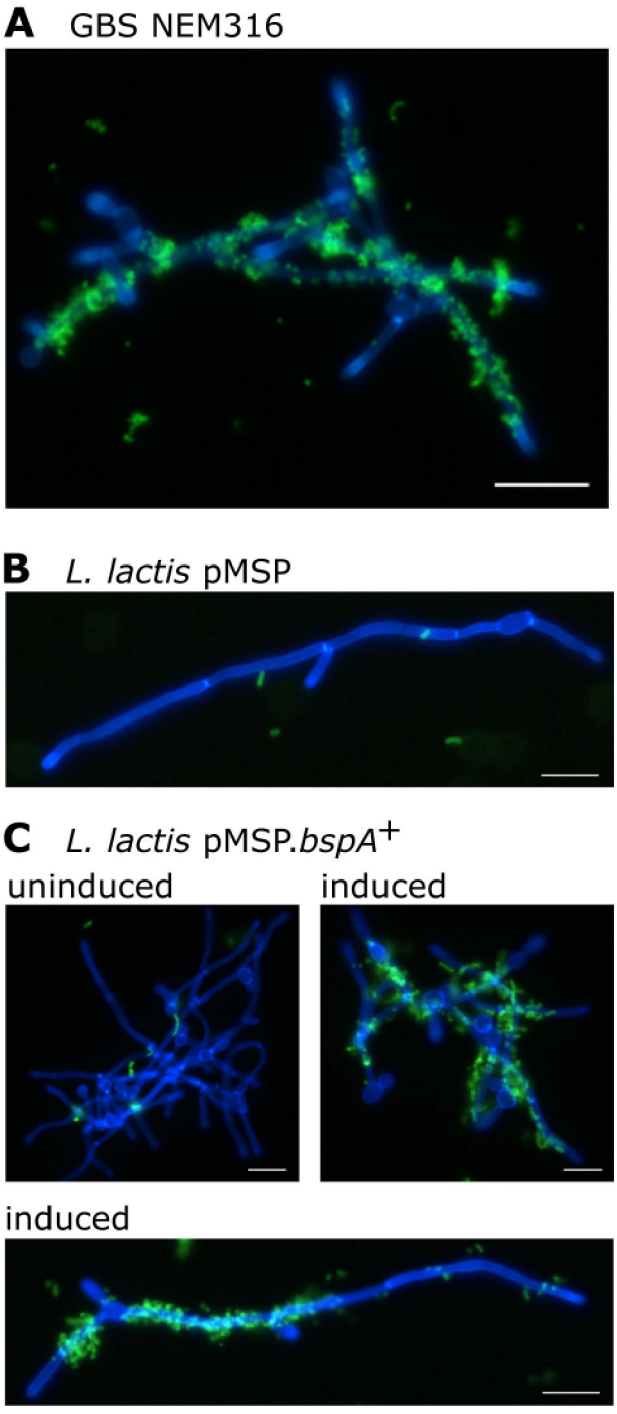
A GBS NEM316
B L. lactis pMSP
C L. lactis pMSP.bspA+
uninduced
induced
induced

FIGURE 5.

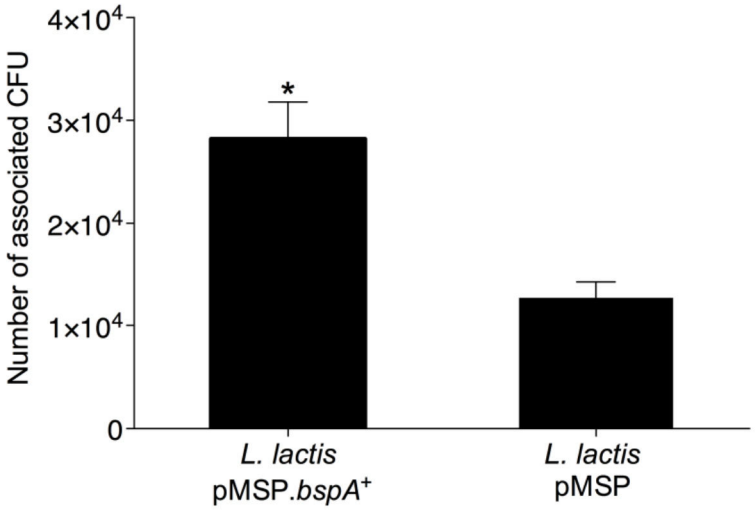
4×10^4
3×10^4
2×10^4
1×10^4
0
Number of associated CFU
*
L. lactis pMSP.bspA+
L. lactis pMSP

FIGURE 6.

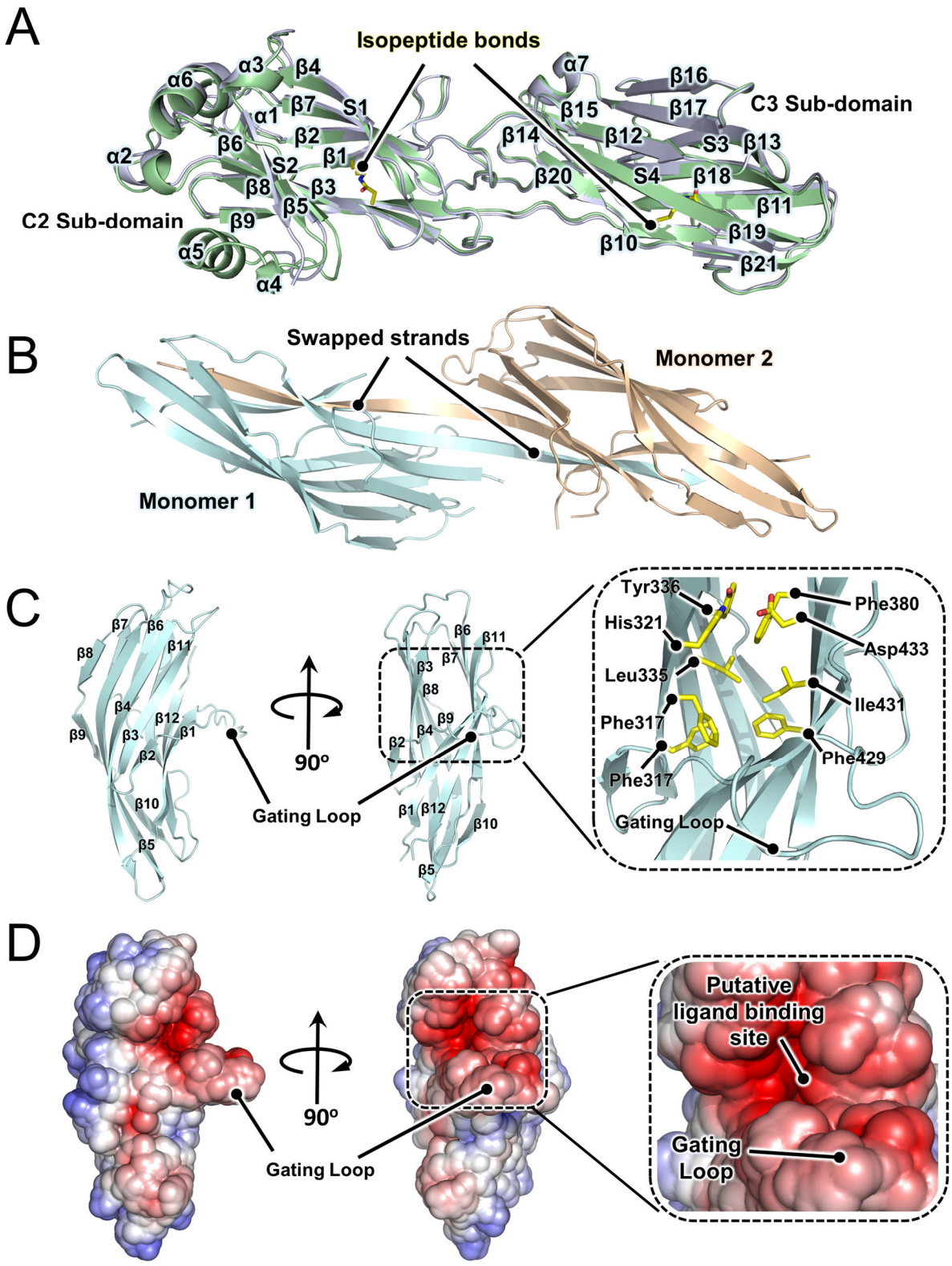
A
Isopeptide bonds
C3 Sub-domain
C2 Sub-domain
α1
α2
α3
α4
α5
α6
α7
β1
β2
β3
β4
β5
β6
β7
β8
β9
β10
β11
β12
β13
β14
β15
β16
β17
β18
β19
β20
β21
S1
S2
S3
S4
B
Swapped strands
Monomer 2
Monomer 1
C
90°
Gating Loop
Tyr336
Phe380
His321
Asp433
Leu335
Ile431
Phe317
Phe429
Phe317
Gating Loop
D
90°
Gating Loop
Putative ligand binding site
Gating Loop

FIGURE 7.

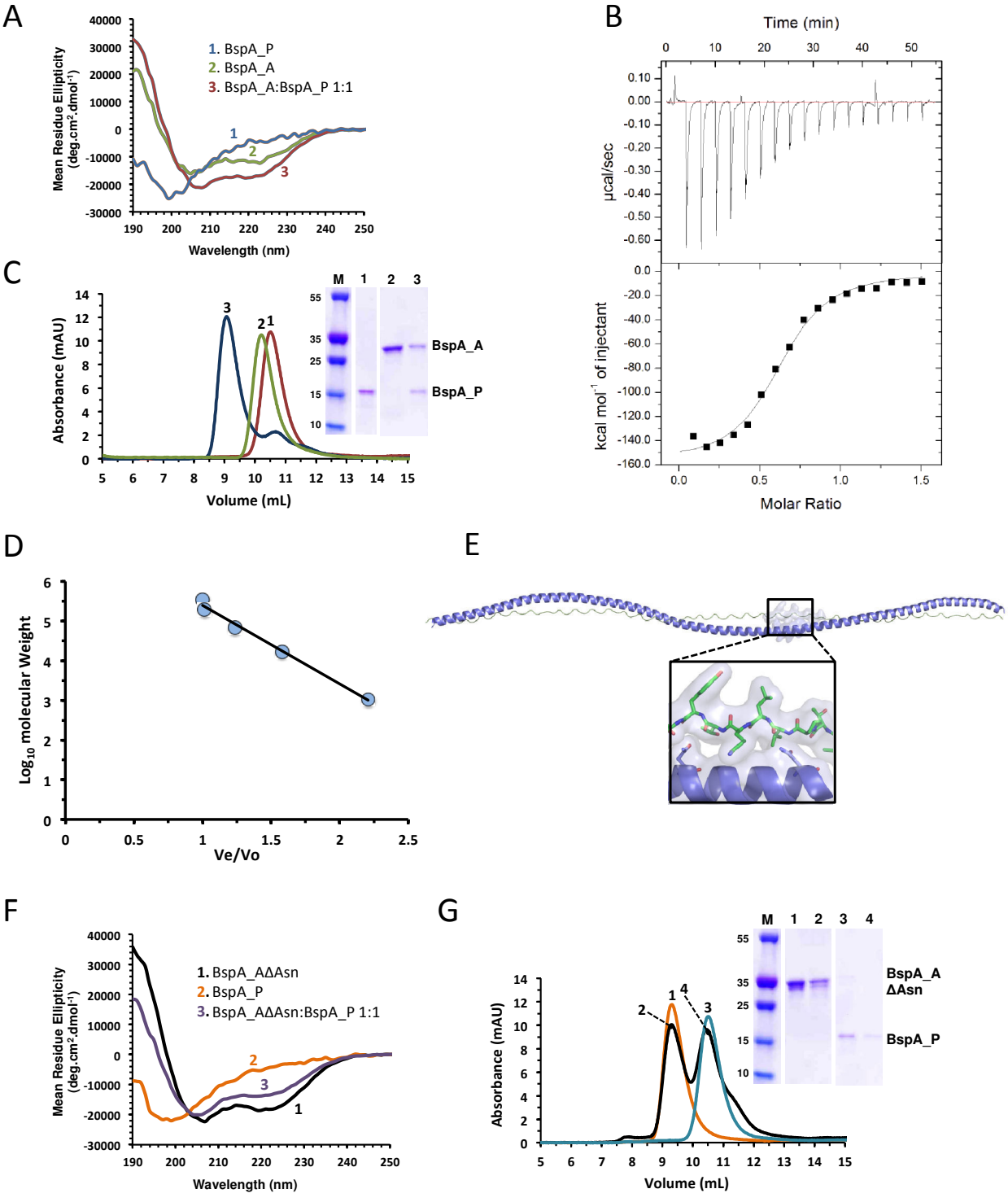
A
Mean Residue Ellipticity (deg.cm².dmol⁻¹)
1. BspA_P
2. BspA_A
3. BspA_A:BspA_P 1:1
Wavelength (nm)
B
Time (min)
µcal/sec
kcal mol⁻¹ of injectant
Molar Ratio
C
Absorbance (mAU)
Volume (mL)
M 1 2 3
BspA_A
BspA_P
D
Log10 molecular Weight
Ve/Vo
E
F
Mean Residue Ellipticity (deg.cm².dmol⁻¹)
1. BspA_AΔAsn
2. BspA_P
3. BspA_AΔAsn:BspA_P 1:1
Wavelength (nm)
G
Absorbance (mAU)
Volume (mL)
M 1 2 3 4
BspA_A ΔAsn
BspA_P

FIGURE 8.

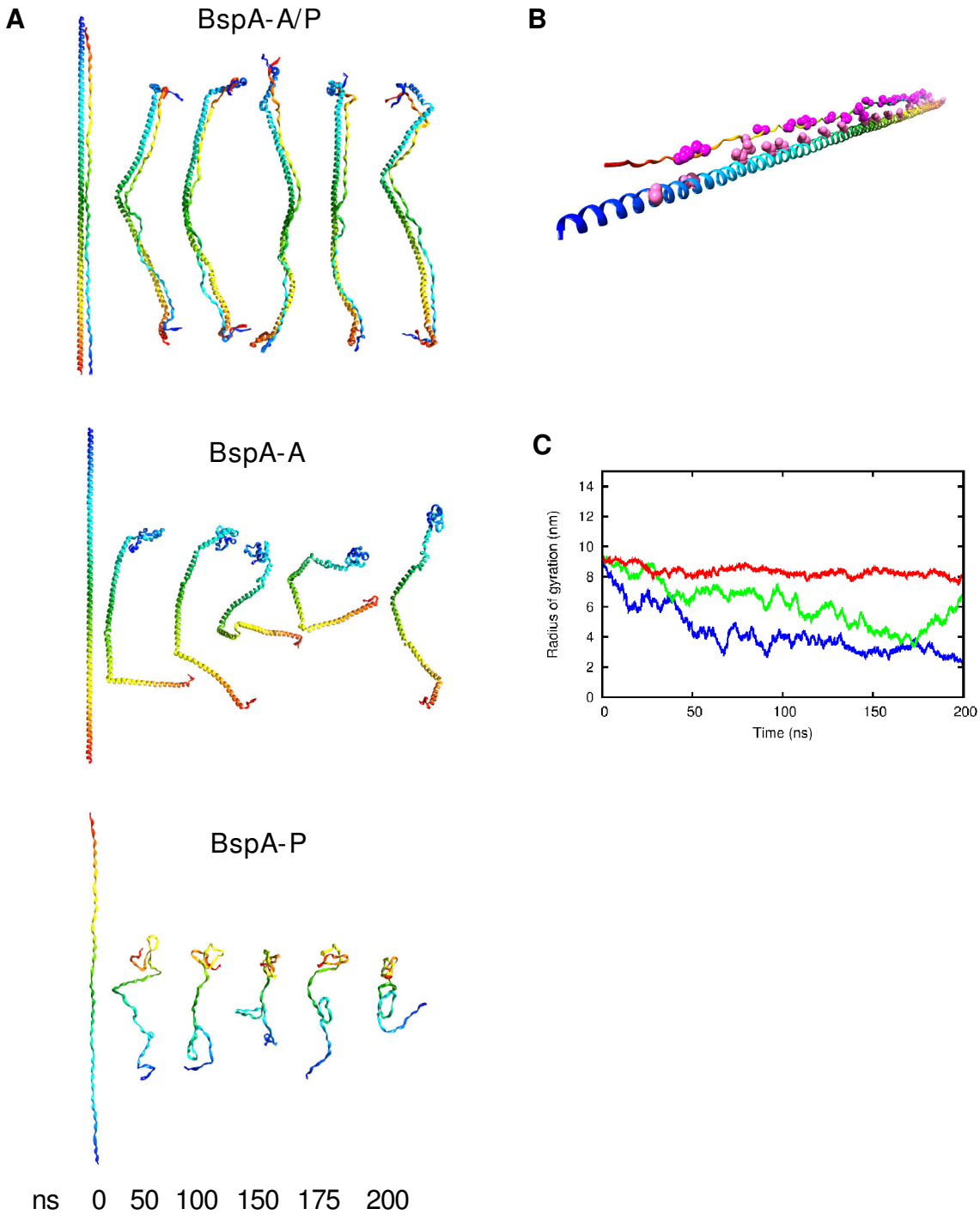
A
BspA-A/P
BspA-A
BspA-P
ns 0 50 100 150 175 200
B
C
Radius of gyration (nm)
Time (ns)
0
2
4
6
8
10
12
14
0
50
100
150
200